

# Ultrafast ratchet dynamics of skyrmion by defect engineering under time-asymmetric magnetic fields

Wei Jin Chen,<sup>1,2,3</sup> Linjie Liu,<sup>2,3</sup> and Yue Zheng<sup>2,3\*</sup>

<sup>1</sup>*School of Materials, Sun Yat-sen University, 510275, Guangzhou, China*

<sup>2</sup>*State Key Laboratory of Optoelectronic Materials and Technologies, Sun Yat-sen University, 510275, Guangzhou, China*

<sup>3</sup>*Micro&Nano Physics and Mechanics Research Laboratory, School of Physics, Sun Yat-sen University, 510275, Guangzhou, China*

The novel ratchet motion of magnetic skyrmions driven by microwave magnetic fields, with the motion direction and speed tunable by field parameters, provides a promising route to drive magnetic skyrmions in materials with poor conductivity. However, as an indirect motion, skyrmion ratchet motion speed is generally low in comparison with the direct motions driven by current. Toward practical applications, it is important to ask if there are mechanisms to realize ultrafast ratchet motion of magnetic skyrmions and how such novel motion can be integrated into racetrack-type skyrmion devices. In this work, we explore the effects of defects and edges on the ratchet motion of magnetic skyrmions driven by time-asymmetric magnetic fields. We demonstrate that the ratchet motion of skyrmion is not only guided along the defect tracks or edges, but also with a remarkable speed-up (with a factor over ten) compared with that in the bulk region. The skyrmion ratchet motion speed reaches 100 m/s along a straight defect track/edge and  $10^9$  rad/s along a circular edge under a field strength of  $\sim$ mT, comparable to those direct motions driven by currents. Moreover, the skyrmion ratchet motion along the defect track/edge can be facilely controlled by the field and defect parameters. Analysis based on time-averaged Thiele's equation of skyrmion verifies that such a speed-up effect is due to the increased time-averaged driving force perpendicular to the skyrmion motion when it approaches the defect track/edge, analogous to that discovered in direct motions driven by currents. The generality of our conclusions has been examined for Bloch and Néel-type skyrmions, for biharmonic and pulsed magnetic fields, and for defect tracks with modified Dzyaloshinskii–Moriya or exchange interactions and anisotropy.

---

\* e-mail: zhengy35@mail.sysu.edu.cn.

Magnetic skyrmions are a kind of particle-like chiral spin textures with a nontrivial topological feature (i.e., cannot be continuously ‘unwound’ to a ferromagnetic or other magnetic states) and a typical size in range of  $10^0\sim 10^2$  nm<sup>1,2</sup>. They have been identified in both conductive and poorly conductive materials possessing Dzyaloshinskii–Moriya interaction (DMI), caused by the breaking of inversion symmetry in crystal lattice<sup>3-8</sup> or nearby the interfaces<sup>9-15</sup>. The relatively small size, robust metastability, as well as the intriguing dynamics and transport properties tunable by various external sources, make magnetic skyrmions appealing building blocks in ultradense information storing and processing devices. Particularly, the concepts of racetrack-type devices are improved by skyrmions, and the threshold current to displace magnetic skyrmions is extremely low compared with magnetic domain walls, implying the potential of developing highly energy-efficient devices.

An in-depth understanding of skyrmion motion characteristics is crucial for their promising applications. It is well-known fact that magnetic skyrmions can be displaced, e.g., by spin polarized currents via the spin-transfer torque (STT) or spin-orbit torque (SOT) applicable for metallic systems<sup>16-18</sup>, and by field or field gradients in the absence of spin torques from the conduction electrons applicable for both metallic and insulating systems<sup>19-26</sup>. The nontrivial topology of skyrmions manifest itself in the motion known as skyrmion Hall effect (SkHE)<sup>27,28</sup>, a reverse effect of the topology-induced emergent fields acting on electrons and magnons. The SkHE would drive skyrmions to the edges of system and causes possible annihilation, limiting the maximum velocity of skyrmion. Meanwhile, when skyrmion is moving along the edges, a speed-up effect occurs due to

the repulsive force of the edge<sup>29,30</sup>. So far, a lot of efforts have been paid to pursue high-speed and controllable motion of skyrmion. Particularly, researchers have proposed the use of racetrack-type structures (e.g., narrow stripes with natural edges or defect tracks with different anisotropy, DMI or exchange interactions from those of the surroundings) to guide the motion of skyrmion<sup>17,30-33</sup>. With the further use of antiferromagnetic bilayer structures<sup>34</sup>, low-symmetry heavy-metal substrates<sup>35</sup> or ferrimagnetic materials<sup>36</sup>, the SkHE can be largely suppressed and the speed limit in skyrmion racetrack devices can be overcome by a factor of ten<sup>35</sup>.

While the academic focus has been put on the direct motion of skyrmion driven by time-unvarying sources, some works have shown that a net motion of skyrmion can be also realized by indirect motion under time-varying sources<sup>23-25,37-39</sup>. Such motions, occurring in systems with space or time asymmetries, are relevant to a general kind of transport phenomena of solitons, named ratchet effect. Remarkably, both the speed and the direction of the skyrmion ratchet motions under time-varying magnetic fields can be tuned by the field parameters<sup>24,39</sup>, indicating a general and feasible strategy to drive skyrmions in both conductive and poorly conductive materials. Nevertheless, being an indirect motion, skyrmion ratchet motion speed is generally low (<10 m/s) compared with the direct motions driven by current, despite relatively fast ratchet motion can be realized via a tradeoff of stability for speed (e.g., by increasing the driving field strength or setting the driving field frequency close to the resonance frequency of skyrmion<sup>24,39</sup>). Toward practical applications, it is important to ask if there are mechanisms to realize ultrafast ratchet motion of skyrmions and how such novel motion can be integrated into

racetrack-type skyrmion devices.

Based on massive micromagnetic simulations and analytical modeling, this work explores the effects of defects and edges on the ratchet motion of magnetic skyrmions driven by time-asymmetric magnetic fields and demonstrates a general mechanism of ultrafast ratchet motion (over 100m/s under a field of ~mT) of magnetic skyrmions via defect engineering. The physical model and the basic idea of defect-induced ultrafast ratchet motion of skyrmion are schematically illustrated in Fig. 1. We consider a novel ratchet motion of skyrmion under driving magnetic fields with a temporal asymmetry<sup>39</sup>. Two kinds of driving fields with temporal asymmetry are focused: in-plane biharmonic magnetic fields  $H_x(t) = H_0[\sin(m\omega t) + \sin(n\omega t + \varphi)]$  with  $m$  and  $n$  being two coprime integers and  $m + n$  being odd, and in-plane pulsed magnetic fields with positive pulses and negative pulses in different magnitudes or widths. Due to the temporal asymmetry of the driving fields, skyrmion can be driven into a net motion even though the time average of driving fields is zero and the system is without any space asymmetry. In the bulk region where the skyrmion is far away from defect tracks or edges, the skyrmion would show ratchet motions with a relatively low speed compared with that near the defect tracks or edges<sup>39</sup>. When the skyrmion approaches to a defect track or an edge, it will be guided along the defect track/edge and the skyrmion ratchet motion exhibits a much larger speed than that in the bulk region. Analogous to that discovered in direct motions driven by currents<sup>29,33</sup>, the speed-up effect of skyrmion ratchet motion can be explained by repulsive interactions (in a time-averaging view) between the skyrmion and the defect track/edge. We will show that the skyrmion ratchet motion speed and

direction along the defect track/edge can be facily controlled by the field and defect parameters. The generality of our conclusions will be examined for Bloch and Néel-type skyrmions, for biharmonic and pulsed magnetic fields, and for defect tracks with modified DMI or exchange interactions and anisotropy.

## Results

### **Defect-mediated skyrmion ratchet motion under time-asymmetric magnetic fields.**

The ratchet effect under time-asymmetric fields is general for both Bloch and Néel-type magnetic skyrmions as they are identical particles from the viewpoint of topology (see Supplementary Fig. S1 and S2). We would take the results of Bloch-type skyrmions to illustrate the key idea of this work. Our simulations are performed on a two-dimensional (2D) Heisenberg-type spin lattice with  $128 \times 128$  sites (see Methods Section for details of the model and values of the model parameters). The temperature-field  $T$ - $H_z$  phase diagram of single-skyrmion state of this spin lattice system is calculated and plotted in Supplementary Fig. S3. It shows that, at a given temperature, the single-skyrmion state (i.e., an isolating skyrmion embedded in a ferromagnetic background) can be stabilized at an intermediate range of the out-of-plane magnetic field  $H_z$ . In the following, we fixed the condition at  $T = 0$  K and  $H_z = 0.015$  (in unit of  $J/g\mu_B$ , see Methods Section). Such a condition stabilizes a skyrmion with diameter of  $\sim 60$  nm if we consider a typical lattice parameter of  $a = 1$  nm. A finite change of temperature and  $H_z$  would not change the main conclusions of this work.

We first reveal the defect-mediated ratchet motion of skyrmion under a biharmonic

magnetic field  $H_x(t) = 0.003[\sin(\omega t) + \sin(3\omega t)]$  along  $x$  axis. The angular frequency of the fields  $\omega$  is set to be 105 rad/s (also in the following). The corresponding frequency is  $f = 16.7$  GHz. This value is close to the resonance frequency of the counter-clockwise (CCW) gyration mode of the skyrmion and leads to a relatively fast ratchet motion<sup>39</sup>. Two cases are investigated. For the first case, denoted as “defect track //  $y$ ”, the  $128a \times 128a$  spin lattice system is in periodic boundary conditions along both  $x$  and  $y$  axes, and a  $4a$ -wide defect track (with the DMI constant being half of that in the bulk region, *i.e.*,  $\eta_{\text{DMI}} = 0.5$ ) parallel to  $y$ -axis is located at  $x = 96a$ . For the second case, denoted as “edge //  $x$ ”, the spin lattice system has a periodic boundary condition along  $x$ -axis and an open-circuit condition along  $y$ -axis (*i.e.*, there are two edges parallel to  $x$ -axis). For both cases, an isolating skyrmion is initially located at the center of the system ( $64a, 64a$ ). The core of skyrmion before motion is far enough from the defect track and edges, therefore the skyrmion motion at the beginning can be considered as that in the bulk region. Figure 2a and 2b respectively depict the motion trajectory of the skyrmion in the two cases. It is clearly seen that for both cases the skyrmion exhibits a ratchet motion with a helical trajectory under the biharmonic in-plane magnetic field. At the beginning, the pitch of the helical trajectory of skyrmion for both cases is rather small (see the “1#” insets in Fig. 2a and 2b), indicating a small ratchet speed. As the skyrmion moves closer to the defect track or the edge, the pitch of the helical trajectory of skyrmion for both cases gradually increases, and becomes much larger than that in the bulk when the skyrmion finally moves along the defect track or the edge (see the “2#” insets in Fig. 2a and 2b). This clearly demonstrates a speed-up effect of the skyrmion ratchet motion caused by

the defect track and edge, analogous to those reported in the direct transport of skyrmion driven by currents<sup>29,33</sup>.

Such a speed-up effect can be quantitatively inferred from the long-time evolution curves of the skyrmion position coordinates  $x_c$  and  $y_c$  of the two cases, as shown in Fig. 2c and 2d, respectively. It shows that the  $y_c$  curve of case “defect track //  $y$ ” and the  $x_c$  curve of case “edge //  $x$ ” have smooth slopes at the beginning of several nanoseconds (the unit of time  $\tau$  is  $\sim 1.5$  ns). This corresponds to the stage of approaching the defect track or edge. Then, the curves show periodic zigzags with steep slopes, corresponding to the stage of high-speed ratchet motion along the defect track or edge. Note, due to the use of periodic boundary conditions, each zigzag of the  $y_c$  or  $x_c$  curve corresponds to a  $128a$  displacement of the skyrmion, and the period of the zigzag is the time for the skyrmion to move over 128 lattices. One can readily estimate the ratchet motion speed  $v_c$  along the defect track and the edge to be about  $68.7a/\tau$  and  $147.9a/\tau$ , respectively. For a typical value of  $a = 1$  nm, the speed values are 45.8 m/s and 98.6 m/s, respectively, which are comparable to that driven by currents. On the other hand, from the slope of the  $y_c$  or  $x_c$  curve at the beginning (see, *e.g.*, in the “1’#” inset in Fig. 2c), the ratchet motion speed in the bulk region to be about  $9.54 a/\tau$  (6.4 m/s for  $a = 1$  nm). This result shows that the speed-up effect of defect track and edge on the skyrmion ratchet motion is remarkable, with a factor over 10.

To clearly see the change of skyrmion configuration under the biharmonic in-plane field and the effect of defect, in Fig. 2e we depict the snapshots of the contour maps of  $m_z$  of case “edge //  $x$ ” during the motion of skyrmion towards and along the edge. The

movies of skyrmion ratchet motion along the defect track and edge are also provided in the Supplementary Information. One can see from these results that, under the driving force of the biharmonic field, the skyrmion is excited into a CCW gyration mode with significant deformation. When it approaches the edge or defect track, the skyrmion has a slight shrinkage of along the direction perpendicular to the edge or defect track. Such a skyrmion-defect interaction reflects that the skyrmion is subjected to a repulsive force from the edge or defect track, in addition to the driving force of the biharmonic field. as we will show later, is crucial for the speed-up effect of skyrmion ratchet motion.

**Facile control on the defect-induced ultrafast ratchet motion of skyrmion.** Note, by varying the phase  $\varphi$  of the biharmonic field in form of  $H_x(t) = h_1 \sin(m\omega t) + h_2 \sin(n\omega t + \varphi)$ , direction of the skyrmion ratchet motion in the bulk region (i.e., away from defect tracks or edges) can be continuously rotated by  $360^\circ$ . Consequently, the skyrmion will be driven towards/along or away from a defect track/edge, depending on the phase  $\varphi$  of the biharmonic field. This  $360^\circ$  net motion of skyrmion controllable by the phase  $\varphi$  is an analogy to the  $360^\circ$  skyrmion motion by controlling the magnetization direction of the spin current injected in the out-of-plane direction<sup>18</sup>, and should be potentially useful in driving skyrmions in insulating systems. Double-track or double-edge structures can be further designed to confine the skyrmion ratchet motion within the region between the double tracks or edges, acting like a racetrack-type highway of the skyrmion ratchet motion. In the following, we discuss the influence of phase  $\varphi$  on the skyrmion ratchet motion within a double-track structure under biharmonic in-plane magnetic fields  $H_x(t)$



$= 0.003[\sin(\omega t) + \sin(3\omega t + \varphi)]$  with  $\varphi$  varying from 0 to  $360^\circ$ . In the simulated  $128a \times 128a$  spin lattice system, two  $4a$ -wide defect tracks (parallel to the  $y$ -axis,  $\eta_{\text{DMI}} = 0.5$ ) are located at  $x = 32a$  and  $x = 96a$ . For a given  $\varphi$ , an isolating skyrmion is initially located at position  $(64a, 64a)$ .

The long-time evolution curves of the position coordinate  $y_c$  and the corresponding trajectories of skyrmion ratchet motion at various phase  $\varphi$  are depicted in Fig. 3a and 3b, respectively. One can see from the number of the zigzags in the  $y_c$  curves in Fig. 3a that the ratchet motion speed of skyrmion along the defect track is sensitive to phase  $\varphi$ . In addition, although the direction of the ratchet motion in the bulk region is  $360^\circ$  (see Supplementary Fig. S4), the skyrmion is finally either in upward ratchet motion along the left defect track  $\parallel y$  or in downward ratchet motion along the right track  $\parallel y$  as shown in Fig. 3b. That is to say, the ratchet motion of skyrmion along the defect track has a fixed direction (*e.g.*, upward along the left defect track  $\parallel y$  and downward along the right defect track  $\parallel y$ ), no matter the skyrmion has an initial upward or downward velocity when it approaches the defect track. Again, this is very much alike the motion of skyrmion trapped along defect tracks or edges driven by current, indicating that the repulsive force of the track plays a dominant role in the ratchet motion of skyrmion.

The skyrmion ratchet motion speed and the speed-up factor as a function of phase  $\varphi$  are calculated and depicted in Fig. 3c, both for motion along the defect track and in the bulk region. Here, the speed along the defect track  $v$  is plotted with plus or minus sign, denoting the upward motion along the left track or downward motion along the right track. Moreover, the speed-up factor is defined as the ratio between the ratchet

motion speed along the defect track (determined by the slope of the zigzag) and that in the bulk region (determined by the slope of the  $y_c$  curves at the beginning 1 ns). One can see that both the ratchet motions in the bulk region and along the defect track are tunable by the phase  $\varphi$ . The  $v$ - $\varphi$  curves are sinusoidal-like, with a near  $40^\circ$  difference between the peaks of the ratchet motion speed along the defect tracks and that of the bulk region. The maximum ratchet motion speed along the defect tracks is about  $91.3a/\tau$  at  $\varphi$  around  $130^\circ$  (downward along the right track) and  $310^\circ$  (upward along the left track), whereas the maximum ratchet motion speed in the bulk region is about  $9.5 a/\tau$  at  $\varphi$  around  $90^\circ$  and  $270^\circ$ . The maximum speed-up factor is over 10 at  $\varphi$  around  $105^\circ$  and  $285^\circ$ , and the minimum is  $\sim 2.2$  at  $\varphi$  around  $35^\circ$  and  $215^\circ$ .

The  $\varphi$ -dependent speed-up effect of the skyrmion ratchet motion along the defect track can be further modified by the defect parameters. Figure 3d depicts the skyrmion ratchet speed  $v_y$  as a function of phase  $\varphi$  of the biharmonic field for cases with different defect strength  $\eta$ . Effect of the width of defect track  $w$  is also shown in the inset. It can be seen that the ratchet motion speed is more sensitive to the defect strength than the width of defect track, implying the dominant effect comes from the border of the defect track. The defect strength mainly affects the ratchet motion speed rather than shifting the  $v$ - $\varphi$  curve. With the increase of the defect strength  $\eta$  from 0.8 to 0.5, the maximum ratchet motion speed increases from about  $68.5a/\tau$  to  $91.3a/\tau$  (by a factor of  $\sim 1.3$ ). Moreover, depinning occurs once the force perpendicular to the defect track exceeds the depinning force but the defect strength is not strong enough ( $\eta = 0.8$ ). The change of width of defect track from  $w = 4a$  to  $12a$  slightly shifts the  $v$ - $\varphi$  curve by  $\sim 15^\circ$ , with

a minor effect on the maximum speed.

To clearly see the effect of phase  $\varphi$  on the skyrmion ratchet motion along the defect tracks, we depict the polar graphs of the skyrmion ratchet motion speed and the speed-up factor as a function of phase  $\varphi$  (Fig. 3e and 3f). The polar curves of ratchet motion speed are in peanut-shape with two peaks and valleys. As the peaks and valleys of polar curve of ratchet motion speed along the defect tracks have a near  $40^\circ$  rotation with those of the bulk region, the polar curve of the speed-up factor shows a distortion from that of the speed curve as shown in Fig. 3f. Note, the motion angle  $\theta$ , which is defined as the angle between the velocity vector and the  $x$ -axis, is  $360^\circ$  rotatable with the change of phase  $\varphi$  when the skyrmion moves in the bulk region. By plotting the polar graphs of the skyrmion ratchet motion speed and the speed-up factor as a function of the motion angle  $\theta$  in the bulk region (Supplementary Fig. S5), one can see that the fastest ratchet motion along the defect track actually occurs when  $\theta$  is about  $0$  and  $180^\circ$ , that is, when the skyrmion is perpendicularly incident to the defect track. For this motion angle, the repulsive force of the defect track is largest, again implying that the important role of the repulsive force of the defect track in the ultrafast ratchet effect.

Skyrmion ratchet motion along the edge is found to be much less sensitive to phase  $\varphi$  of the biharmonic in-plane magnetic fields than the case of motion along defect track (see Supplementary Fig. S6 and S7). In the simulation, there are two open edges at the two boundaries of the lattice systems parallel to  $x$ -axis as that shown in Fig. 2b. With phase  $\varphi$  changing from  $0^\circ$  to  $360^\circ$ , the direction of the skyrmion ratchet motion is either along the upper edge (rightward motion) or along the bottom edge (leftward motion).

Moreover, the ratchet motion speed along the edge is generally large, which is about  $150a/\tau$  for all  $\varphi$  and is about 1.7 times of the maximum speed moving along the defect track ( $\sim 90a/\tau$ ). The ultrafast ratchet motion along the edge indicates a strong repulsive force exerted by the edge, and the much weaker phase-sensitivity in contrast to the case of defect track is believed to be caused by much more intensive excitation of spin waves nearby the edge, with an intensity insensitive to phase  $\varphi$ . For this case, it would be more efficient to tune the ratchet motion speed along the edge by controlling the field strength of the biharmonic field, or by controlling the pulse width of pulsed magnetic fields as shown in Fig. 4. Here, the pulsed fields  $H_x(t)$  are repetitive sequences of alternating positive pulse over a time  $TN_1$  and negative pulse over a time  $TN_2$  (Fig. 4a). The field strength of the positive and negative pulses is 0.003 in reduced unit ( $\sim 3.3\text{mT}$ ), and  $TN_1 + TN_2 = TN$  is fixed to be  $0.04\tau$  (i.e.,  $\sim 60\text{ ps}$ ). From the long-time evolution curves of the position coordinate  $x_c$  of skyrmion ratchet motion at various  $TN_1$  (Fig. 4b), one can see that the skyrmion ratchet motion speed along the edge significantly increases with the change of  $TN_1$  from  $0.002\tau$  to  $0.01\tau$ . Such a facile control of the ratchet motion speed by pulsed fields is believed to be caused by the resonant effect and is practically useful for driving skyrmion along edges.

### **Mechanism analysis of the defect-induced ultrafast ratchet motion of skyrmion.**

To understand the origin of the defect-induced ultrafast ratchet motion of skyrmion, we further make an analysis on the skyrmion motion based on the time-averaged Thiele's equation. It should be pointed out that, under the effect of time-varying magnetic fields,

the skyrmion system is excited with fast spin modes (magnons) and the skyrmion shows significant dynamic deformations. This drives the skyrmion transport beyond the rigid-particle approximation, and it is necessary to consider the skyrmion-magnon interaction. Here, making use of the periodic property of the driving magnetic field and the fact that the spin modes relax much faster than the translation mode, one can adopt a similar idea of previous works<sup>21,23</sup> to derive a time-averaged Thiele's equation for the ratchet motion of skyrmion (see Methods Section for the details). The time-averaged Thiele's equation is still in classic form as  $\mathbf{G} \times \mathbf{v} + \mathbf{D} \mathbf{v} = -\mathbf{F}$ , where  $\mathbf{v}$  and  $\mathbf{F}$  are the time-averaged velocity and driving force, and  $\mathbf{G}$  and  $\mathbf{D}$  being the gyromagnetic vector and the dissipative force tensor determined by the time-averaged magnetization, respectively. The driving force  $\mathbf{F}$  includes the contribution of the external field, the repulsive force exerted by the defect track or edge, as well as the skyrmion-magnon interaction (see Eq. (16) in the Methods Section).

Figure 5a depicts the snapshots of the force density maps when a skyrmion moves toward and along an edge parallel to  $x$ -axis under a biharmonic in-plane magnetic field  $H_x(t) = H_0[\sin(\omega t) + \sin(3\omega t)]$  with  $\omega = 105$  rad/s and  $H_0 = 0.003$  in reduced unit. The skyrmion is initially at position  $(64a, 64a)$  in the  $128a \times 128a$  simulation spin lattice. One can see that the force density takes large values mainly near the skyrmion. When the skyrmion approaches the edges, the force changes direction from being lower-right to being perpendicular to the edge, and with a remarkable increase of magnitude (see, the ranges of the color bars). To see the difference between the forces subjected by the skyrmion when it moves in the bulk region and along a defect track or edge, we further

depict in Fig. 5b the evolution curves of time-averaged driving force components  $F_{x(y)}$  subjected by skyrmion when it moves in the bulk region (“bulk”), along a defect track parallel to  $y$ -axis (“defect track //  $y$ ”), and along an edge parallel to  $x$ -axis (“edge //  $x$ ”), driven by the same biharmonic in-plane magnetic field. For the case of “defect track //  $y$ ”, two  $4a$ -wide defect tracks (parallel to the  $y$ -axis,  $\eta_{\text{DMI}} = 0.5$ ) are located at  $x = 32a$  and  $x = 96a$ . For the case of “edge //  $x$ ”, the spin lattice has two edges parallel to  $x$ -axis. Our result shows that the driving force is small for ratchet motion without defect tracks or edges (case “bulk”) or far from the defect tracks or edges (cases “defect track //  $y$ ” and “edge //  $x$ ” at the beginning). Moreover, the driving force shows a remarkable increase when the skyrmion approaches the defect track or edge. At steady motion, the driving force is found to be (in unit of  $J_0a/\hbar$ )  $\mathbf{F} = (F_x, F_y) = (-7.3 \times 10^{-3}, -6.3 \times 10^{-3})$  for case “bulk”,  $(-5.5 \times 10^{-2}, -4.9 \times 10^{-3})$  for case “defect track //  $y$ ”, and  $(1.0 \times 10^{-2}, -1.4 \times 10^{-1})$  for case “edge //  $x$ ”, respectively. One can estimate the ratchet motion speed  $v$  and angle  $\theta$  of the three cases according to these values of the driving force and the approximated relation  $\mathbf{G} \times \mathbf{v} \sim -\mathbf{F}$ , and by taking  $|\mathbf{G}| \sim 4\pi$ . This gives  $v = 7.67a/\tau$  and  $\theta = 311^\circ$  for case “bulk”,  $v = 43.8a/\tau$  and  $\theta = 275^\circ$  for case “defect track //  $y$ ”, and  $v = 111.4a/\tau$  and  $\theta = 4.36^\circ$  for case “edge //  $x$ ”. These estimated values are in good consistence with the simulation results, verifying the correctness of our physical picture. Therefore, it can be concluded that the speed-up effect of skyrmion ratchet motion by defect tracks or edges is caused by the remarkable increase of the net driving force perpendicular to the skyrmion motion when it approaches the defect track or edge (Fig. 5c).

Note, there are actually various situations when a skyrmion encounters the defect

track/edge as schematically shown in Fig. 5d. Depending on the relative magnitudes of the force perpendicular to the defect track/edge  $F$  subjected by skyrmion and the critical force  $F_c$  of depinning or annihilation, three situations of skyrmion motion can happen: (i) skyrmion moves along the defect track or edge ( $F < F_c$ ), (ii) passes through the defect track or edge ( $F > F_c$  of depinning), and (iii) annihilates at the defect track or edge ( $F > F_c$  of annihilation). The  $F_c$  of a defect track should be a function of the defect strength and track width<sup>40</sup>.

Based on the above force analysis, we can further explain the facile controllability of the speed-up effect along the defect track or edge by the field and defect parameters. Here we take the skyrmion ratchet motion along defect track //  $y$  under biharmonic fields  $H_x(t) = 0.003[\sin(\omega t) + \sin(3\omega t + \varphi)]$  as an example. In previous result (Fig. 3 and Fig. 4), we have shown that the ratchet motion along the defect track are tunable by the phase  $\varphi$  and the defect strength  $\eta$ . Figure 5e depicts the time-averaged driving force components  $F_{x(y)}$  subjected by skyrmion as a function of phase  $\varphi$ . Figure 5f shows a plot of the skyrmion ratchet speed  $v_y$  as a function of  $F_x$ . One can see that the peak and valley values of the ratchet motion speed actually corresponds to the maximum and minimum values of  $F_x$ . There is a clear linear correlation between  $v_y$  and  $F_x$ , with a slope of  $4\pi$ , in consistent with the approximated relation  $\mathbf{G} \times \mathbf{v} \sim -\mathbf{F}$ .

## Discussion

The ultrafast ratchet motions can be realized along defect tracks which have a different exchange interaction or anisotropy strength from that of the bulk region (as shown in

Supplementary Fig. S8 and Fig. S9). Moreover, an ultrafast rotation motion of skyrmion can be realized when the skyrmion is confined within a circular disk (Supplementary Fig. S10), with the angular velocity being over  $10^9$  rad/s. More complicate motions of skyrmion can realized by proper defect engineering, geometrical designing, and control of the field parameters. The same mechanism is also applicable for Néel-type skyrmions (see, Supplementary Fig. S11). The reported ultrafast skyrmion ratchet motion is a conjoint effect of the soliton-like feature of magnetic skyrmions and skyrmion-defect interaction or the skyrmion-edge interaction. The driving sources can be magnetic fields or other time-varying sources with gigahertz characteristic frequencies rather than spin polarized currents. The reported mechanism therefore provides a general and feasible strategy to efficiently drive skyrmion in both metallic and insulating systems.

To conclude, we found that while skyrmion exhibits a  $360^\circ$  ratchet motion in the bulk region under time-asymmetric magnetic fields, it will be guided along the defect tracks and edges when it is close to them, with the appearance of a remarkable speed-up effect. Moreover, the ratchet motion speed is comparable to that driven by currents. The speed-up effect is controllable by the field and defect parameters and is caused by the increased time-averaged driving force perpendicular to the skyrmion motion when it approaches the defect track/edge.

## Methods

**Micromagnetic simulation.** The motion of an isolated skyrmion in a chiral magnet with bulk DM interaction is numerical studied. Basing on a Heisenberg model on a two-



dimensional square lattice, we write the following effective Hamiltonian of a chiral magnet as

$$\mathcal{H}(\mathbf{m}_i) = -J \sum_{\langle i,j \rangle} \mathbf{m}_i \cdot \mathbf{m}_j - D \left( \sum_i \mathbf{m}_i \times \mathbf{m}_{i+e_x} \cdot \hat{e}_x + \sum_i \mathbf{m}_i \times \mathbf{m}_{i+e_y} \cdot \hat{e}_y \right) - \sum_i \mathbf{H}(t) \cdot \mathbf{m}_i \quad (1)$$

where  $\mathbf{m}_i$  is the magnetization vector at site  $i$ ,  $J$  is the Heisenberg exchange coefficient,  $D$  is the DM interaction coefficient, and  $\mathbf{H}(t) = \mathbf{H}_0 + \mathbf{h}(t)$  is the external magnetic field which is the sum of a constant field normal to the plane  $\mathbf{H}_0 = (0, 0, H_z)$  and a time-varying in-plane field  $\mathbf{h}(t)$ .

The dynamics of skyrmion is captured by solving the stochastic Landau-Lifshitz-Gilbert (LLG) equation,

$$\frac{d\mathbf{m}_i}{dt} = -\gamma \left[ \mathbf{m}_i \times (\mathbf{H}_i^{\text{eff}} + \mathbf{L}_i^{\text{fl}}(t)) \right] + \alpha \left( \mathbf{m}_i \times \frac{d\mathbf{m}_i}{dt} \right) \quad (2)$$

or in the equivalent form,

$$\frac{d\mathbf{m}_i}{dt} = -\frac{\gamma}{\alpha^2 + 1} \left[ \mathbf{m}_i \times (\mathbf{H}_i^{\text{eff}} + \mathbf{L}_i^{\text{fl}}(t)) + \alpha \mathbf{m}_i \times \left[ \mathbf{m}_i \times (\mathbf{H}_i^{\text{eff}} + \mathbf{L}_i^{\text{fl}}(t)) \right] \right] \quad (3)$$

where  $\gamma = g\mu_B / \hbar$  is the gyromagnetic ratio,  $\alpha$  is the Gilbert damping coefficient,  $\mathbf{H}_i^{\text{eff}}$  is the effective magnetic field given by  $\mathbf{H}_i^{\text{eff}} = -\partial \mathcal{H} / \partial \mathbf{m}_i$ , and  $\mathbf{L}_i^{\text{fl}}(t)$  is the stochastic field caused by the effects of a thermally fluctuating environment interacting with  $\mathbf{m}_i$ .  $\mathbf{L}_i^{\text{fl}}(t)$  satisfies  $\langle \mathbf{L}_i^{\text{fl}}(t) \rangle = 0$  and  $\langle L_{i\beta}^{\text{fl}}(t) L_{i\lambda}^{\text{fl}}(s) \rangle = \alpha k_B T \gamma^{-1} m^{-1} \delta_{ij} \delta_{\beta\lambda} \delta(t-s)$ , where  $\beta$  and  $\lambda$  are Cartesian indices,  $T$  is temperature,  $k_B$  is the Boltzmann constant, and  $m = |\mathbf{m}_i| = |g\mu_B| / a^3$  is the norm of the magnetization vector.

Numerical simulations based on the stochastic LLG equation are performed via an explicit Euler iteration scheme. The size of sample systems is fixed to be  $128 \times 128$  sites under the periodic boundary condition. The Heisenberg exchange  $J$  is taken to be  $J/k_B$

= 50 K, and the strength of the DM interaction coefficient is  $D = 0.15J$ . The spin turn angle  $\theta$  in the helical structure is  $\sim 6^\circ$  as determined by  $\theta = \arctan[D/(\sqrt{2}J)]$ . The Gilbert damping coefficient  $\alpha$  is taken to be 0.1. The external magnetic field normal to the plane is fixed to be  $H_z = 0.015$ , in unit of  $J/(g\mu_B)$ , which is  $\sim 0.16$  T for  $g$  equal to 6.74. The time step is taken to be 0.01, in unit of  $\hbar/J$ , which is  $\sim 1.5$  fs. In the main text, the time is expressed in the reduced form  $\tilde{t} = t/\tau$ , with  $\tau$  being  $10^3 \hbar/J \approx 1.5$  ns. To first obtain the steady skyrmion, the magnetic structure of the spin lattice system is initially set with a downward magnetization in the center region and with an upward magnetization elsewhere and is relaxed over a sufficiently long time ( $>3$  ns).

To characterize the skyrmion, we calculate the topological charge density,

$$q = \frac{1}{4\pi} \mathbf{m} \cdot (\partial_x \mathbf{m} \times \partial_y \mathbf{m}) \quad (4)$$

as defined in the continuous form. The total topological charge is then given by

$$Q = \int q dx dy \quad (5)$$

And the position of skyrmion  $\mathbf{R} = (x_c, y_c)$  can be determined by

$$x_c = \frac{\int x q dx dy}{Q}, \quad y_c = \frac{\int y q dx dy}{Q} \quad (6)$$

**Analytical model of skyrmion ratchet motion.** Consider the steady ratchet motion of skyrmion driven by a periodically oscillating magnetic field. In this case, spin waves (magnons) are excited and deforms the skyrmion dynamically, and the conventional Thiele's equation based on the rigid-particle model needs to be modified. Assume that the characteristic frequency of the driving field is in order of gigahertz, which is much lower than that of the spin waves (magnons). The magnetization distribution of a

skyrmion can be written as the sum of a slowly-varying part and fast-varying part<sup>21,23</sup>,

$$\mathbf{m}(\mathbf{r}, t) = \mathbf{m}_0 + \mathbf{n} \quad (7)$$

where  $\mathbf{m}_0$  is the slowly-varying part and  $\mathbf{n}$  is the fast-varying part related to the magnons, respectively.  $\mathbf{m}_0$  can be approximated by the equilibrium magnetization of skyrmion, and its time-dependence is related to the skyrmion position  $\mathbf{R}(t)$  as  $\mathbf{m}_0 = \mathbf{m}_0(\mathbf{r} - \mathbf{R}(t))$ .

Substituting the above  $\mathbf{m}(\mathbf{r}, t)$  into the LLG equation (see, Eq. (2)), one obtains

$$-(\dot{\mathbf{R}} \cdot \nabla) \mathbf{m}_0 + \dot{\mathbf{n}} = -\gamma \mathbf{m} \times \mathbf{H}_{\text{eff}} + \alpha (\mathbf{m}_0 + \mathbf{n}) \times (-(\dot{\mathbf{R}} \cdot \nabla) \mathbf{m}_0 + \dot{\mathbf{n}}) \quad (8)$$

Multiplying  $\mathbf{m}_0 \cdot \left( \frac{\partial \mathbf{m}_0}{\partial x_i} \times \right)$  on all the terms of the above equation gives

$$\begin{aligned} & -\mathbf{m}_0 \cdot \left( \frac{\partial \mathbf{m}_0}{\partial x_i} \times (\dot{\mathbf{R}} \cdot \nabla) \mathbf{m}_0 \right) + \mathbf{m}_0 \cdot \left( \frac{\partial \mathbf{m}_0}{\partial x_i} \times \dot{\mathbf{n}} \right) \\ & = -\gamma \mathbf{m}_0 \cdot \left( \frac{\partial \mathbf{m}_0}{\partial x_i} \times (\mathbf{m} \times \mathbf{H}_{\text{eff}}) \right) - \alpha \mathbf{m}_0 \cdot \left( \frac{\partial \mathbf{m}_0}{\partial x_i} \times (\mathbf{m}_0 \times (\dot{\mathbf{R}} \cdot \nabla) \mathbf{m}_0) \right) + \\ & \quad \alpha \mathbf{m}_0 \cdot \left( \frac{\partial \mathbf{m}_0}{\partial x_i} \times (\mathbf{n} \times (-(\dot{\mathbf{R}} \cdot \nabla) \mathbf{m}_0)) \right) + \alpha \mathbf{m}_0 \cdot \left( \frac{\partial \mathbf{m}_0}{\partial x_i} \times (\mathbf{m} \times \dot{\mathbf{n}}) \right) \end{aligned} \quad (9)$$

By defining

$$\mathbf{g} = \left[ \mathbf{m}_0 \cdot \left( \frac{\partial \mathbf{m}_0}{\partial y} \times \frac{\partial \mathbf{m}_0}{\partial z} \right), \mathbf{m}_0 \cdot \left( \frac{\partial \mathbf{m}_0}{\partial z} \times \frac{\partial \mathbf{m}_0}{\partial x} \right), \mathbf{m}_0 \cdot \left( \frac{\partial \mathbf{m}_0}{\partial x} \times \frac{\partial \mathbf{m}_0}{\partial y} \right) \right] \quad (10)$$

and

$$\vec{\mathbf{d}} = \begin{bmatrix} d_{11} & d_{12} & d_{13} \\ d_{21} & d_{22} & d_{23} \\ d_{31} & d_{32} & d_{33} \end{bmatrix}, \quad d_{ij} = \frac{\partial m_{0k}}{\partial x_i} \frac{\partial m_{0k}}{\partial x_j} \quad (11)$$

Eq. (10) can be further written as

$$\begin{aligned} \mathbf{g} \times \dot{\mathbf{R}} + \vec{\mathbf{d}} \cdot \dot{\mathbf{R}} & = -\gamma \mathbf{m}_0 \cdot \left( \frac{\partial \mathbf{m}_0}{\partial x_i} \times (\mathbf{m} \times \mathbf{H}_{\text{eff}}) \right) - \mathbf{m}_0 \cdot \left( \frac{\partial \mathbf{m}_0}{\partial x_i} \times \dot{\mathbf{n}} \right) + \\ & \quad \alpha \mathbf{m}_0 \cdot \left( \frac{\partial \mathbf{m}_0}{\partial x_i} \times (\mathbf{n} \times (-(\dot{\mathbf{R}} \cdot \nabla) \mathbf{m}_0)) \right) + \alpha \mathbf{m}_0 \cdot \left( \frac{\partial \mathbf{m}_0}{\partial x_i} \times (\mathbf{m} \times \dot{\mathbf{n}}) \right) \end{aligned} \quad (12)$$

The time averages of those terms related to  $\mathbf{n}$  and  $\dot{\mathbf{n}}$  in the above equation can be neglected. This leads to

$$\mathbf{g} \times \langle \dot{\mathbf{R}} \rangle + \vec{\mathbf{d}} \cdot \langle \dot{\mathbf{R}} \rangle = - \left\langle \gamma \mathbf{m}_0 \cdot \left( \frac{\partial \mathbf{m}_0}{\partial x_i} \times (\mathbf{m} \times \mathbf{H}_{\text{eff}}) \right) \right\rangle \quad (13)$$

By integrating all the terms of the Eq. (13) with space coordinates, one finally obtains

$$\mathbf{G} \times \langle \dot{\mathbf{R}} \rangle + \alpha \vec{\mathbf{D}} \cdot \langle \dot{\mathbf{R}} \rangle = \mathbf{F} \quad (14)$$

Here  $\langle \rangle$  denotes time averaging over a period. The effective force is defined by

$$F_i = \int -\gamma \mathbf{m}_0 \cdot \left( \frac{\partial \mathbf{m}_0}{\partial x_i} \times \langle \mathbf{m} \times \mathbf{H}_{\text{eff}} \rangle \right) dV \quad (15)$$

where

$$\langle \mathbf{m} \times \mathbf{H}_{\text{eff}} \rangle \approx \langle A \mathbf{n} \times \nabla^2 \mathbf{n} - D \mathbf{n} \times (\nabla \times \mathbf{n}) + \mathbf{n} \times \mathbf{h}(t) \rangle \quad (16)$$

with the first term corresponding to the contribution of magnons. The ratchet motion speed  $\mathbf{v} \equiv \langle \dot{\mathbf{R}} \rangle$  can be analytically obtained by solving the dynamic motion equation of skyrmion, i.e., Eq. (14).

## Data availability

The data presented in the current study are available from the corresponding authors on reasonable request.

## References

1. Nagaosa, N., & Tokura, Y. Topological properties and dynamics of magnetic skyrmions. *Nature Nanotechnology*, **8**, 899 (2013).

2. Fert, A., Reyren, N., & Cros, V. Magnetic skyrmions: advances in physics and potential applications. *Nature Reviews Materials*, **2**, 1-15 (2017).
3. Roessler, U. K., Bogdanov, A. N., & Pfleiderer, C. Spontaneous skyrmion ground states in magnetic metals. *Nature*, **442**, 797-801 (2006).
4. Mühlbauer S, Binz B, Jonietz F, et al. Skyrmion lattice in a chiral magnet. *Science*, **323**, 915-919 (2009).
5. Münzer W, Neubauer A, Adams T, et al. Skyrmion lattice in the doped semiconductor Fe<sub>1-x</sub>Co<sub>x</sub>Si. *Physical Review B*, **81**, 041203 (2010).
6. Pfleiderer C, Adams T, Bauer A, et al. Skyrmion lattices in metallic and semiconducting B20 transition metal compounds. *Journal of Physics: Condensed Matter*, **22**, 164207 (2010).
7. Adams T, Chacon A, Wagner M, et al. Long-wavelength helimagnetic order and skyrmion lattice phase in Cu<sub>2</sub>OSeO<sub>3</sub>. *Physical Review Letters*, **108**, 237204 (2012).
8. Ruff E, Widmann S, Lunkenheimer P, et al. Multiferroicity and skyrmions carrying electric polarization in GaV<sub>4</sub>S<sub>8</sub>. *Science Advances*, **1**, e1500916 (2015).
9. Heinze S, Von Bergmann K, Menzel M, et al. Spontaneous atomic-scale magnetic skyrmion lattice in two dimensions. *Nature Physics*, **7**, 713-718 (2011).
10. Jiang W, Upadhyaya P, Zhang W, et al. Blowing magnetic skyrmion bubbles. *Science*, **349**, 283-286 (2015).
11. Boulle O, Vogel J, Yang H, et al. Room-temperature chiral magnetic skyrmions in ultrathin magnetic nanostructures. *Nature Nanotechnology*, **11**, 449 (2016).
12. Woo S, Litzius K, Krüger B, et al. Observation of room-temperature magnetic

skyrmions and their current-driven dynamics in ultrathin metallic ferromagnets.

*Nature Materials*, **15**, 501-506 (2016).

13. Moreau-Luchaire C, Moutafis C, Reyren N, et al. Additive interfacial chiral interaction in multilayers for stabilization of small individual skyrmions at room temperature. *Nature Nanotechnology*, **11**, 444 (2016).
14. Wang L, Feng Q, Kim Y, et al. Ferroelectrically tunable magnetic skyrmions in ultrathin oxide heterostructures. *Nature Materials*, **17**, 1087-1094 (2018).
15. Meng K Y, Ahmed A S, Baćani M, et al. Observation of nanoscale skyrmions in SrIrO<sub>3</sub>/SrRuO<sub>3</sub> bilayers. *Nano Letters*, **19**, 3169-3175 (2019).
16. Iwasaki J, Mochizuki M, Nagaosa N. Current-induced skyrmion dynamics in constricted geometries. *Nature Nanotechnology*, **8**, 742 (2013).
17. Sampaio J, Cros V, Rohart S, et al. Nucleation, stability and current-induced motion of isolated magnetic skyrmions in nanostructures. *Nature Nanotechnology*, **8**, 839-844 (2013).
18. Tomasello R, Martinez E, Zivieri R, et al. A strategy for the design of skyrmion racetrack memories. *Scientific Reports*, **4**, 6784 (2014).
19. Liu Y H, Li Y Q, Han J H. Skyrmion dynamics in multiferroic insulators. *Physical Review B*, **87**, 100402 (2013).
20. Everschor K, Garst M, Binz B, et al. Rotating skyrmion lattices by spin torques and field or temperature gradients. *Physical Review B*, **86**, 054432 (2012).
21. Kong L, Zang J. Dynamics of an insulating skyrmion under a temperature gradient. *Physical Review Letters*, **111**, 067203 (2013).

22. Upadhyaya P, Yu G, Amiri P K, et al. Electric-field guiding of magnetic skyrmions. *Physical Review B*, **92**, 134411 (2015).
23. Wang W, Beg M, Zhang B, et al. Driving magnetic skyrmions with microwave fields. *Physical Review B*, **92**, 020403 (2015).
24. Moon K W, Kim D H, Je S G, et al. Skyrmion motion driven by oscillating magnetic field. *Scientific Reports*, **6**, 20360 (2016).
25. Psaroudaki C, Loss D. Skyrmions driven by intrinsic magnons. *Physical Review Letters*, **120**, 237203 (2018).
26. Wang C, Xiao D, Chen X, et al. Manipulating and trapping skyrmions by magnetic field gradients. *New Journal of Physics*, **19**, 083008 (2017).
27. Jiang W, Zhang X, Yu G, et al. Direct observation of the skyrmion Hall effect. *Nature Physics*, **13**, 162-169 (2017).
28. Litzius K, Lemesh I, Krüger B, et al. Skyrmion Hall effect revealed by direct time-resolved X-ray microscopy. *Nature Physics*, **13**, 170-175 (2017).
29. Iwasaki J, Koshibae W, Nagaosa N. Colossal spin transfer torque effect on skyrmion along the edge. *Nano Letters*, **14**, 4432-4437 (2014).
30. Zhang X, Zhao G P, Fangohr H, et al. Skyrmion-skyrmion and skyrmion-edge repulsions in skyrmion-based racetrack memory. *Scientific Reports*, **5**, 7643 (2015).
31. Fert A, Cros V, Sampaio J. Skyrmions on the track. *Nature Nanotechnology*, **8**, 152-156 (2013).
32. Tomasello R, Martinez E, Zivieri R, et al. A strategy for the design of skyrmion racetrack memories. *Scientific Reports*, **4**, 6784 (2014).

33. Castell-Queralt J, González-Gómez L, Del-Valle N, et al. Accelerating, guiding, and compressing skyrmions by defect rails. *Nanoscale*, **11**, 12589-12594 (2019).
34. Zhang X, Zhou Y, Ezawa M. Magnetic bilayer-skyrmions without skyrmion Hall effect. *Nature Communications*, **7**, 1-7 (2016).
35. Göbel B, Mook A, Henk J, et al. Overcoming the speed limit in skyrmion racetrack devices by suppressing the skyrmion Hall effect. *Physical Review B*, **99**, 020405 (2019).
36. Woo S, Song K M, Zhang X, et al. Current-driven dynamics and inhibition of the skyrmion Hall effect of ferrimagnetic skyrmions in GdFeCo films. *Nature Communications*, **9**, 1-8 (2018).
37. Reichhardt C, Ray D, Reichhardt C J O. Magnus-induced ratchet effects for skyrmions interacting with asymmetric substrates. *New Journal of Physics*, **17**, 073034 (2015).
38. Ma X, Reichhardt C J O, Reichhardt C. Reversible vector ratchets for skyrmion systems. *Physical Review B*, **95**, 104401(2017).
39. Chen W, Liu L, Ji Y, et al. Skyrmion ratchet effect driven by a biharmonic force. *Physical Review B*, **99**, 064431(2019).
40. Navau, C., Del-Valle, N., & Sanchez, A. Interaction of isolated skyrmions with point and linear defects. *Journal of Magnetism and Magnetic Materials*, **465**, 709-715 (2018).

## **Acknowledgements**



The authors gratefully acknowledge the financial support of National Natural Science Foundation of China (Nos. 11972382, 11672339, 11832019), Guangzhou Science and Technology Project (No. 201707020002), and Fundamental Research Funds for the Central Universities.

### **Author contributions**

Y.Z. initiated and performed this work and manuscript. W.J.C. conceived and designed the basic idea, structures. W.J.C. performed the simulations and modeling. W.J.C., L.J.L. and Y.Z. analyzed the results and co-wrote the manuscript. All authors contributed to discussion and reviewed the manuscript.

### **Competing interests**

The authors declare no competing interests.

### **Additional information**

Supplementary information is available for this paper at <https://doi.org/xxx>.

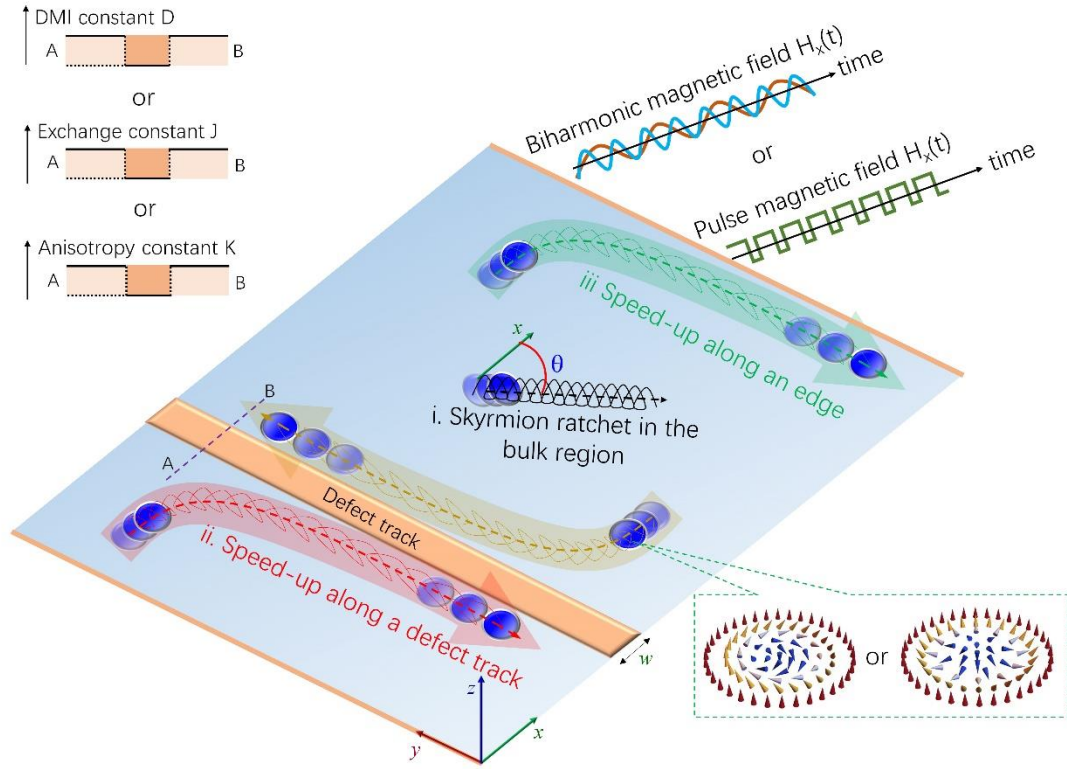


**Fig. 1 Schematic illustrations of the physical model and the basic idea of defect-induced ultrafast ratchet motion of skyrmion under time-asymmetric magnetic fields.** Analogy to other soliton systems, both Bloch and Néel type magnetic skyrmions would be driven into ratchet motions by time-varying forces with temporal asymmetry, e.g., in-plane biharmonic magnetic fields  $H_x(t) = H_0[\sin(m\omega t) + \sin(n\omega t + \varphi)]$  with  $m$  and  $n$  being two coprime integers and  $m + n$  being odd, or in-plane pulsed magnetic fields with positive pulses and negative pulses in different magnitudes or widths. In the bulk region (i.e., free of defects or edges), the speed of such ratchet motions is relatively low, though a continuous control of speed and direction of such ratchet motions can be achieved by tuning the field parameters (e.g., the frequency  $\omega$ , phase  $\varphi$  and strength  $H_0$  of the biharmonic field, width of the pulsed field, etc.). When the skyrmion approaches to a defect track (with a different DMI, exchange or anisotropy from that of the bulk region) or an edge, it will be guided along the defect track/edge and the skyrmion ratchet motion exhibits a remarkable speed-up in comparison with that in the bulk region, due to the remarkably increase of the time-averaged driving force perpendicular to the skyrmion motion when it approaches the defect track/edge. Furthermore, the skyrmion ratchet motion speed and direction along the defect track/edge can be facilely controlled by the field and defect parameters.

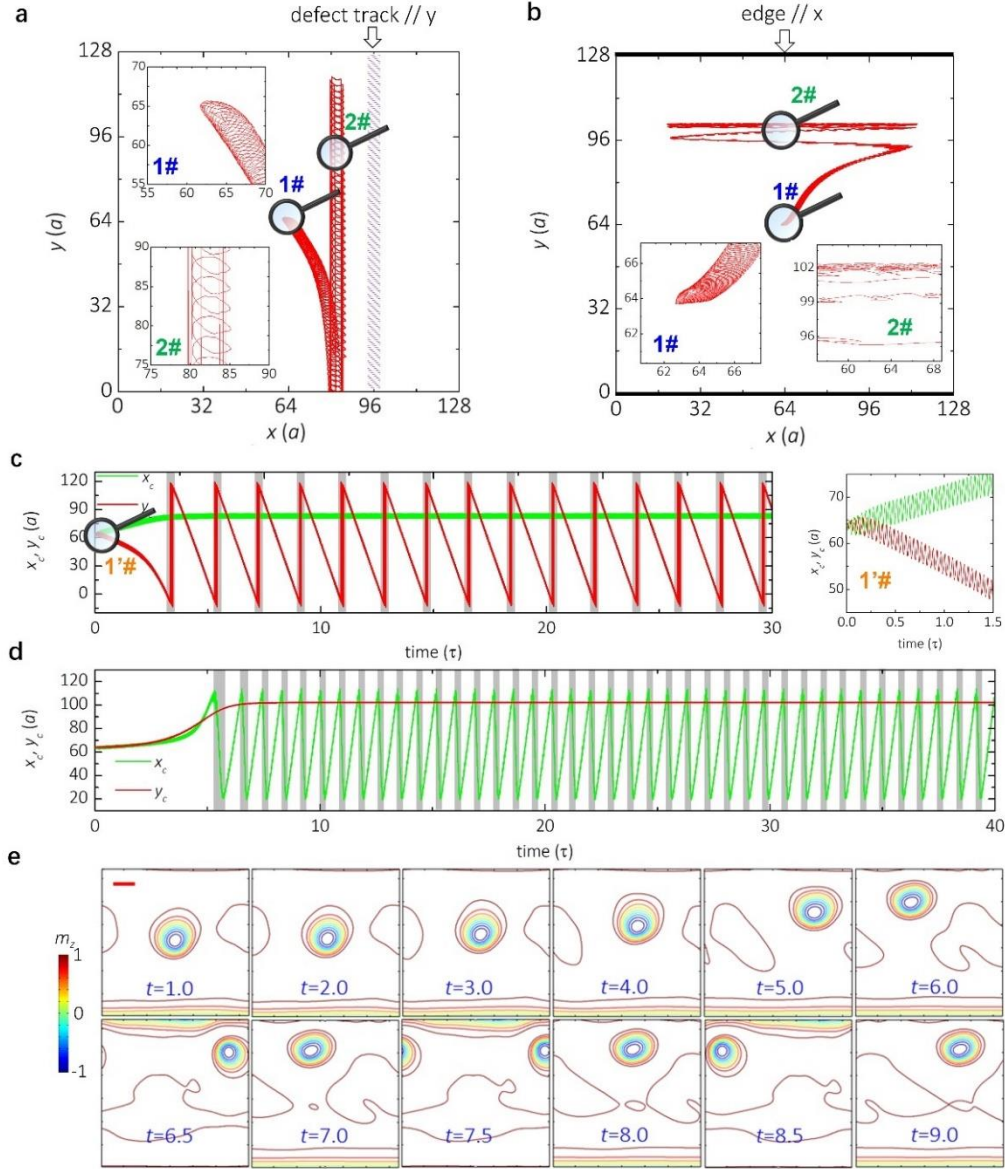


**Fig. 2 Long-time defect-mediated skyrmion ratchet motion under a biharmonic in-plane magnetic field  $H_x(t) = 0.003[\sin(\omega t) + \sin(3\omega t)]$ .** **a** Trajectory of a skyrmion moving toward and along a 4a-wide defect track ( $\eta_{\text{DMI}} = 0.5$ ) parallel to the y-axis (denoted as “defect track // y”) and locating at  $x = 96a$ . **b** Trajectory of a skyrmion moving toward and along an edge parallel to the x-axis (denoted as “defect track // x”) and locating at  $y = 128a$ . To clearly see the speed-up effect, for both cases, the skyrmion is initially located at position  $(64a, 64a)$ , which is far enough from the defect track and edge, so that the skyrmion motion therein can be considered as in the bulk region. **c, d** Corresponding long-time evolution curves of the skyrmion position coordinates  $x_c$  and  $y_c$  of cases **a** and **b**. **e** Snapshots of the contour maps of  $m_z$  of case **b**, from which the skyrmion configuration can be clearly seen. In **a-d**, the skyrmion position  $(x_c, y_c)$  is determined by  $x_c = \int x q dx dy / Q$  and  $y_c = \int y q dx dy / Q$ , where  $q$  is the topological charge density and  $Q = \int q dx dy$  is the topological charge. The skyrmion position nearby the boundaries is problematic due to the periodic boundary condition of the simulation box.

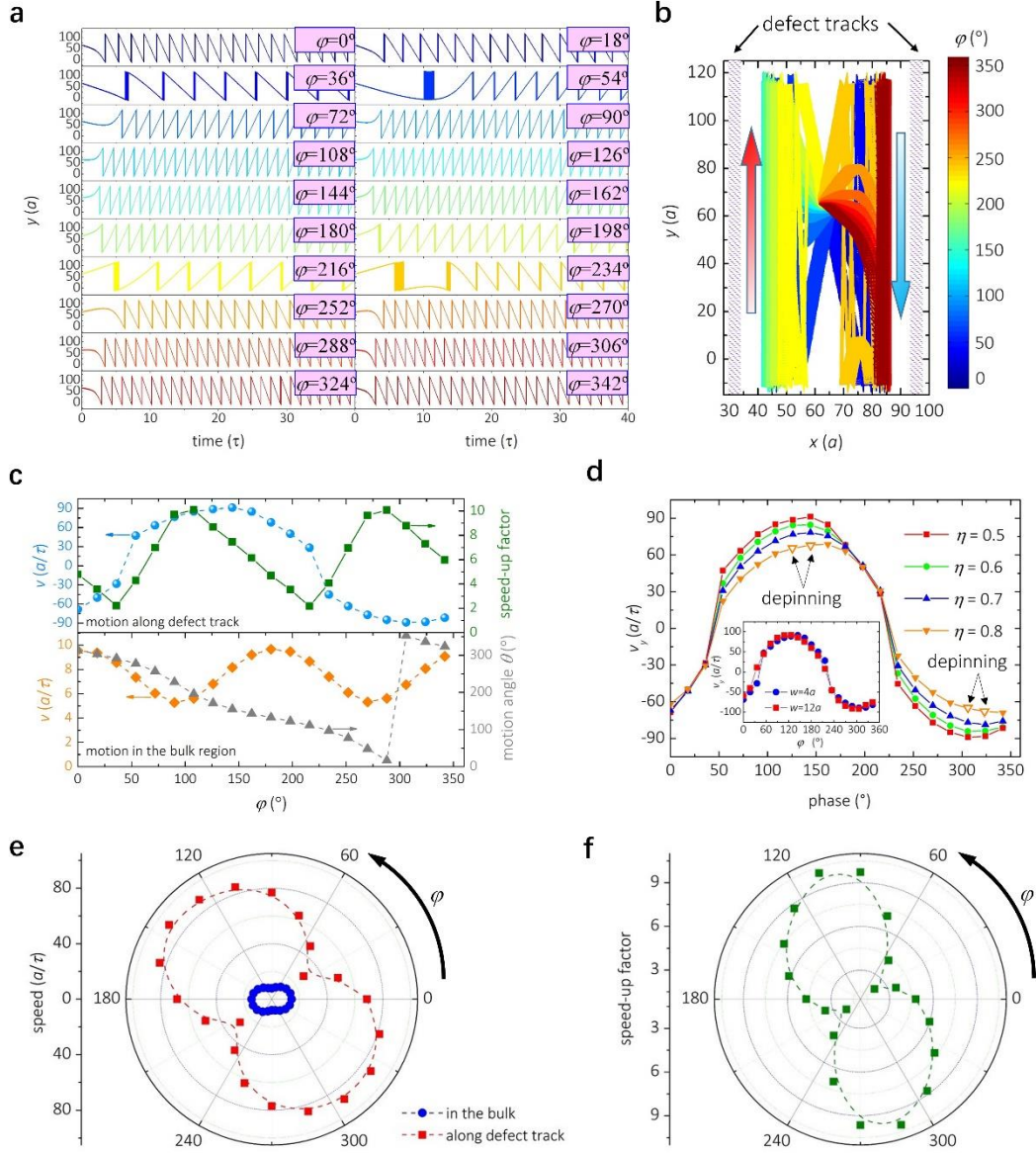


**Fig. 3 The influence of phase  $\varphi$  on the skyrmion ratchet motion along defect tracks // y under biharmonic in-plane magnetic fields  $H_x(t) = 0.003[\sin(\omega t) + \sin(3\omega t + \varphi)]$ .** **a** Long-time evolution curves of the position coordinate  $y_c$  of skyrmion ratchet motion controlled by phase  $\varphi$ . In the simulation box, two  $4a$ -wide defect tracks (parallel to the  $y$ -axis,  $\eta_{\text{DMI}} = 0.5$ ) are located at  $x = 32a$  and  $x = 96a$ . For a given  $\varphi$ , the skyrmion is initially located at position  $(64a, 64a)$  and the skyrmion motion at the beginning can be considered as in the bulk region. Under the driving of  $H_x(t)$ , the skyrmion will be finally either in upward ratchet motion along the left defect track //  $y$  or in downward ratchet motion along the right track //  $y$ , depending on the value of phase  $\varphi$ . **b** Trajectories of skyrmion ratchet motion at various phase  $\varphi$ . **c** Comparison of the skyrmion ratchet motion velocity along the defect track //  $y$  and in the bulk region. In the bulk region, the ratchet motion speed is approximately a sinusoidal function of phase  $\varphi$  in period of  $180^\circ$ , with a maximum value of about  $\sim 10a/\tau$ . Moreover, the ratchet direction (denoted by the motion angle  $\theta$ ) is rotatable over  $360^\circ$  by changing  $\varphi$ . For the ratchet motion

along the defect track, the motion direction is either upward or downward along the defect track, and the speed is approximately a sinusoidal function of phase  $\varphi$  in period of  $360^\circ$  with a maximum value of about  $\sim 90a/\tau$ . The speed-up factor is denoted as the ratio of the ratchet motion speed along the defect track to that in the bulk region. It is an oscillating function of phase  $\varphi$  in period of  $180^\circ$  with a maximum value of  $\sim 10$  as shown in the up panel. **d** Skyrmion ratchet speed  $v_y$  as a function of phase  $\varphi$  of the biharmonic field for the case of “defect track // y” with different defect strength  $\eta$ . Effect of the width of defect track is shown in the inset. Note, depinning occurs once the force perpendicular to the defect track exceeds the depinning force but the defect strength is not strong enough ( $\eta = 0.8$ ). **e** Skyrmion ratchet motion speed and **f** speed-up factor as a function of phase  $\varphi$ . The speed in the bulk region is determined by the  $y_c$  curves at the beginning 1 ns.



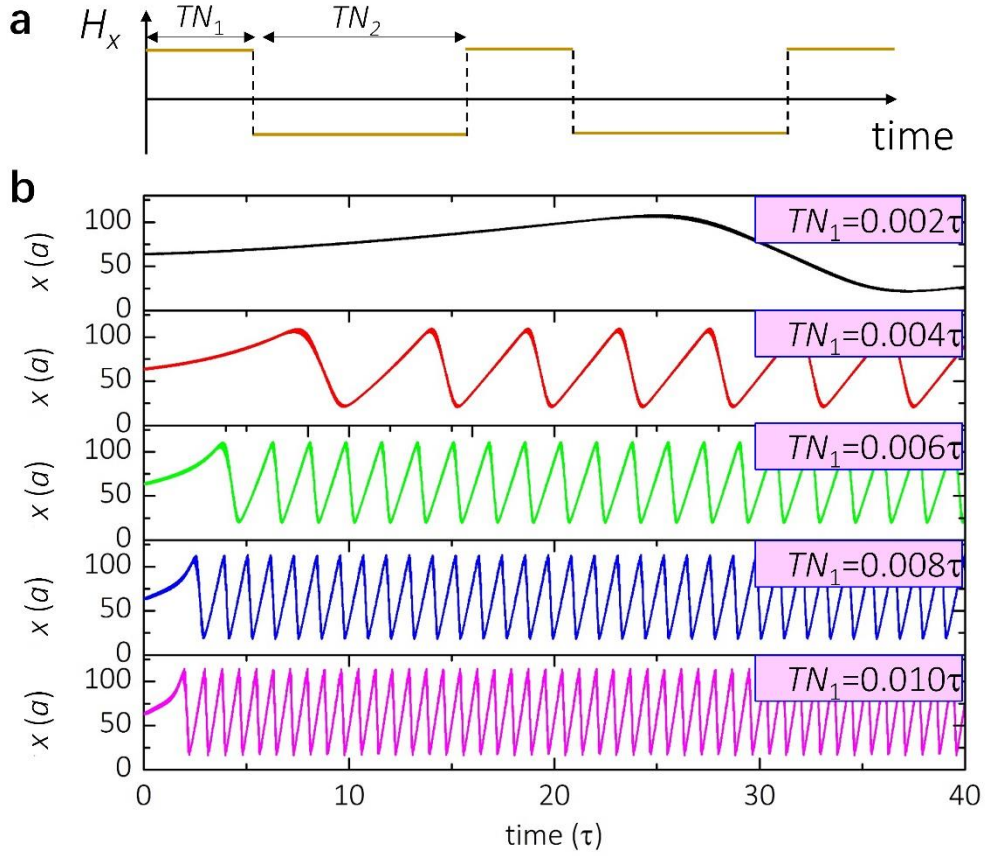


**Fig. 4 Ultrafast skyrmion ratchet motion along edges //  $x$  under pulsed in-plane magnetic fields.** **a** Schematic of the pulsed fields  $H_x(t)$ , which are repetitive sequences of alternating positive pulse over a time  $TN_1$  and negative pulse over a time  $TN_2$ . **b** Long-time evolution curves of the position coordinate  $x_c$  of skyrmion ratchet motion at various  $TN_1$ . Here, the magnitudes of the positive and negative pulses are  $0.003J/g\mu_B$ , and  $TN_1 + TN_2 = TN$  is fixed to be 60 ps.

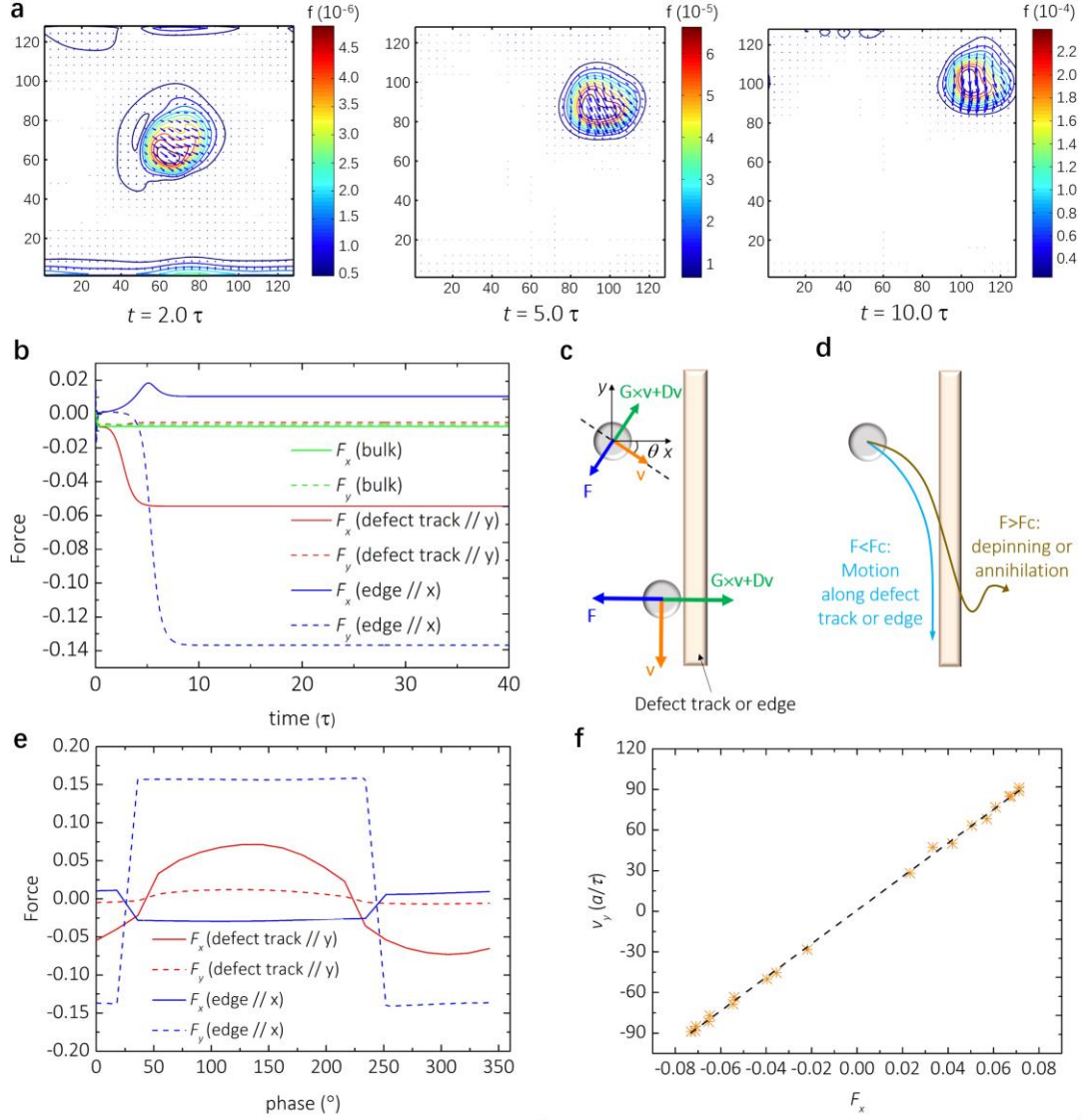


**Fig. 5 Force analysis of the defect-induced ultrafast ratchet motion of skyrmion under biharmonic in-plane magnetic fields  $H_x(t) = 0.003[\sin(\omega t) + \sin(3\omega t + \phi)]$ .** **a** Snapshots of the force density maps of skyrmion moving toward and along an edge parallel to  $x$ -axis. **b** Evolution of time-averaged driving force components  $F_{x(y)}$  subjected by skyrmion when it moves in the bulk region (denoted as “bulk”), along a defect track parallel to  $y$ -axis (denoted as “defect track //  $y$ ”), and along an edge parallel to  $x$ -axis (denoted as “edge //  $x$ ”). For all the cases, the box size is  $128a \times 128a$ , and skyrmion is initially located at position  $(64a, 64a)$ . For the case of “defect track //  $y$ ”, the defect track is  $4a$ -wide with  $\eta_{\text{DMI}} = 0.5$  and located at  $x = 96a$ . For the case of “edge //  $x$ ”, the edge is located at  $y = 128a$ . **c** Schematic of the forces subjected by a skyrmion when it is moving in the bulk region and along a defect track or edge. **d** Schematic illustration of two situations when a skyrmion encounters a defect track or edge. Depending on the relative magnitudes of the force perpendicular to the defect track/edge  $F$  subjected by skyrmion and the critical force  $F_c$  of depinning or annihilation, three situations of skyrmion motion are expected: (i) skyrmion moves along the defect track or edge ( $F < F_c$ ), (ii) passes through the defect track or edge ( $F >$

$F_c$  of depinning), and (iii) annihilates at the defect track or edge ( $F > F_c$  of annihilation).  
**e** Time-averaged driving force components  $F_{x(y)}$  subjected by skyrmion as a function of phase  $\varphi$  of the biharmonic field for the case of “defect track // y”. **f** The linear correlation between the skyrmion ratchet speed  $v_y$  and  $F_x$  for the case of “defect track // y”.



Supplimentary Information for

**Ultrafast ratchet dynamics of skyrmion by defect engineering under time-asymmetric magnetic fields**

Weijin Chen,<sup>1,2,3</sup> Linjie Liu,<sup>2,3</sup> and Yue Zheng<sup>2,3\*</sup>

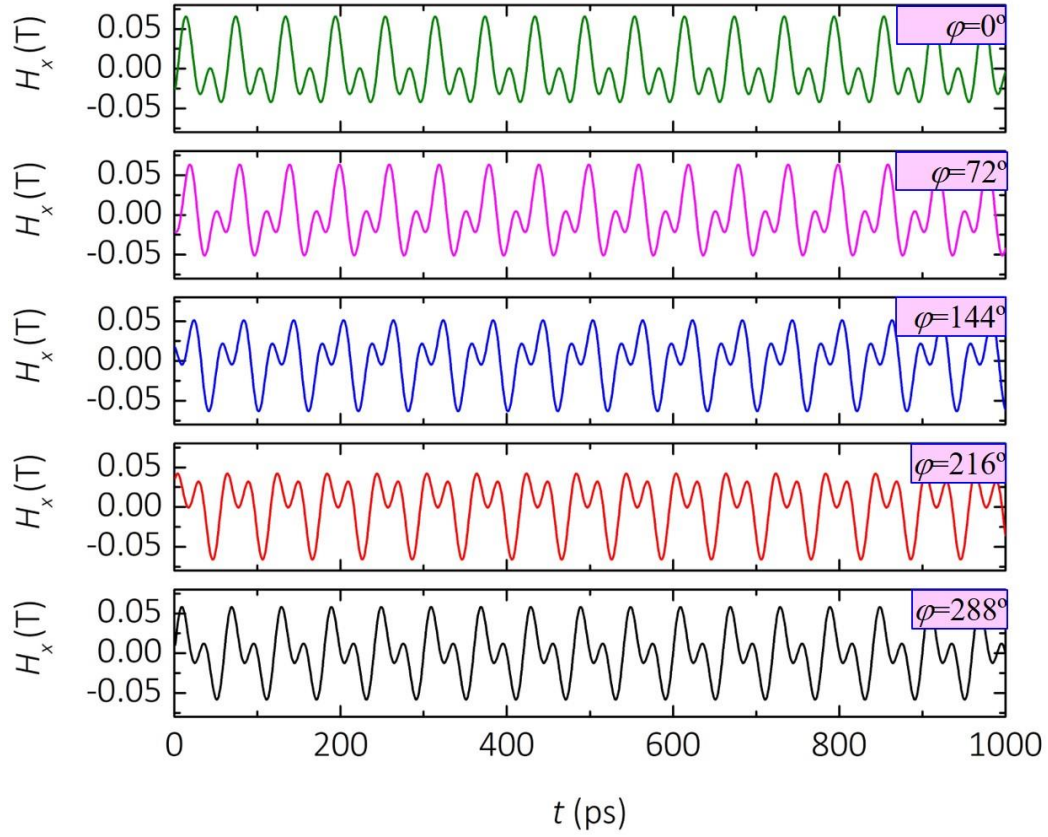
<sup>1</sup>*School of Materials, Sun Yat-sen University, 510275, Guangzhou, China*

<sup>2</sup>*State Key Laboratory of Optoelectronic Materials and Technologies, Sun Yat-sen University, 510275, Guangzhou, China*

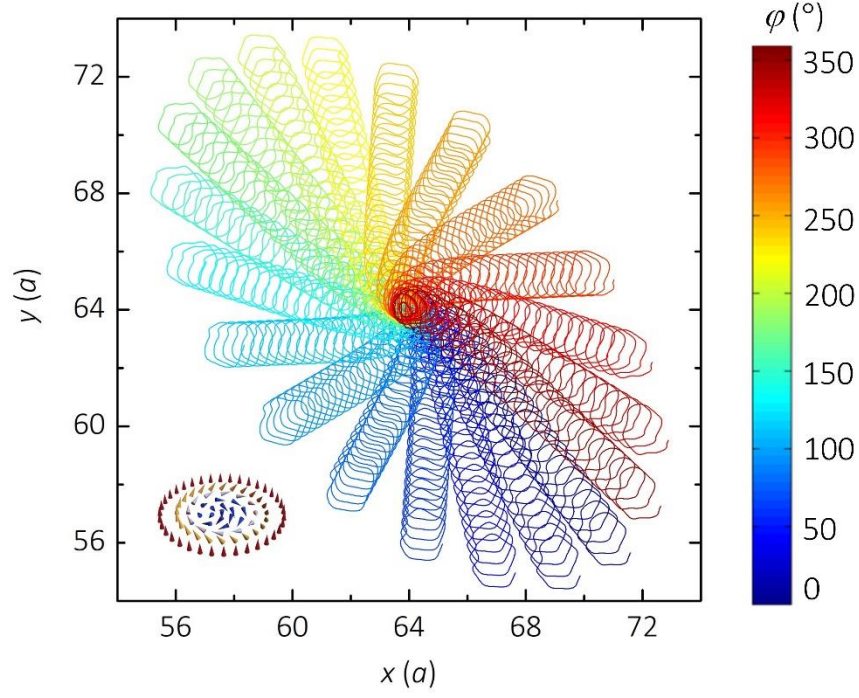
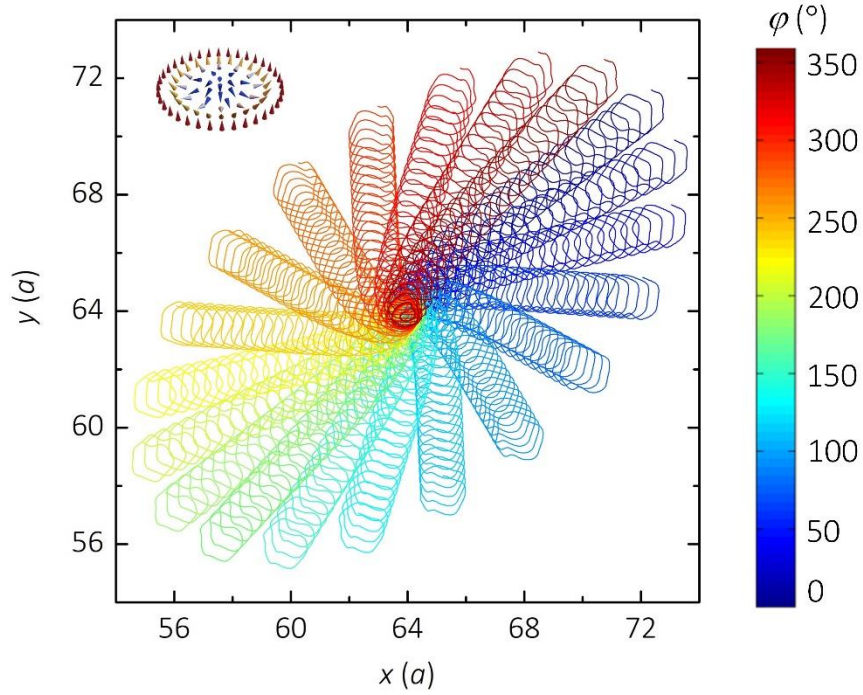
<sup>3</sup>*Micro&Nano Physics and Mechanics Research Laboratory, School of Physics, Sun Yat-sen University, 510275, Guangzhou, China*

---

\* e-mail: zhengy35@mail.sysu.edu.cn.



**Fig. S1 The biharmonic in-plane magnetic fields  $H_x(t) = H_0[\sin(\omega t) + \sin(3\omega t + \varphi)]$  as functions of time at different  $\varphi$ .** The angular frequency of the fields  $\omega$  is set to be 105 rad/s and  $H_0 = 0.003 J/g\mu_B \approx 0.033$  T.

**a****b**

**Fig. S2 Skyrmion ratchet motion under the biharmonic in-plane magnetic fields  $H_x(t) = 0.003[\sin(\omega t) + \sin(3\omega t + \varphi)]$  at different  $\varphi$  in the absence of defects or edges. **a** Bloch-type skyrmion and **b** Neél-type skyrmion. Trajectories of skyrmion ratchet motion at various phase  $\varphi$  are given in different colors. For a given  $\varphi$ , the skyrmion is initially located at position  $(64a, 64a)$ .**

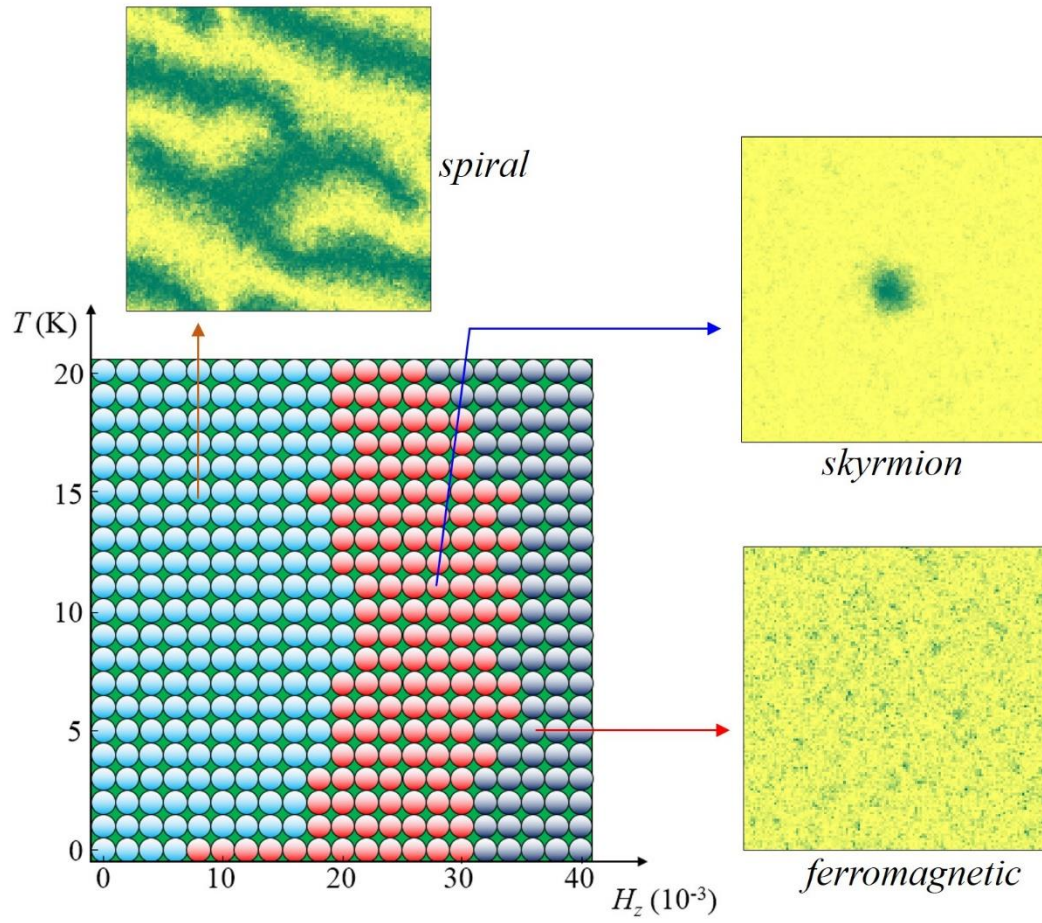


**Fig. S3 Temperature-field  $T$ - $H_z$  phase diagram of single-skyrmion state.** The phase diagram is obtained by performing LLG simulations at various temperature  $T$  and out-of-plane magnetic field  $H_z$  on a  $128 \times 128$  spin lattice with a single-skyrmion state being the trivial state. At a given temperature, the single-skyrmion state can be stabilized at an intermediate range of  $H_z$ . At smaller  $H_z$ , the spiral state is more stable. At larger  $H_z$ , the ferromagnetic state is more stable.

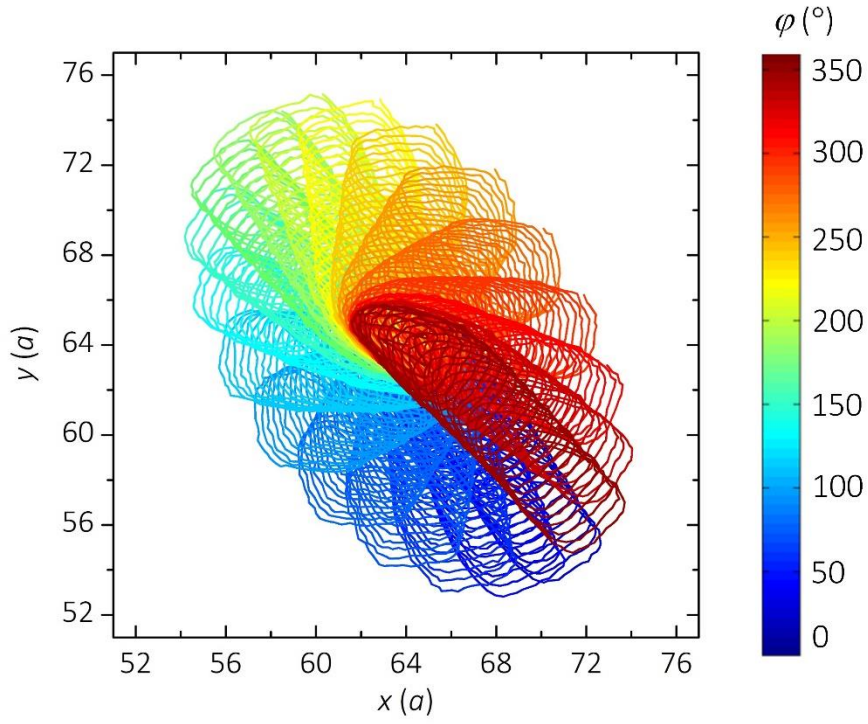


**Fig. S4 Skyrmion ratchet motion in the bulk region under biharmonic in-plane magnetic fields  $H_x(t) = 0.003[\sin(\omega t) + \sin(3\omega t + \phi)]$ .** Trajectories of skyrmion ratchet motion at various phase  $\phi$  are given in different colors. For a given  $\phi$ , the skyrmion is initially located at position  $(64a, 64a)$ .



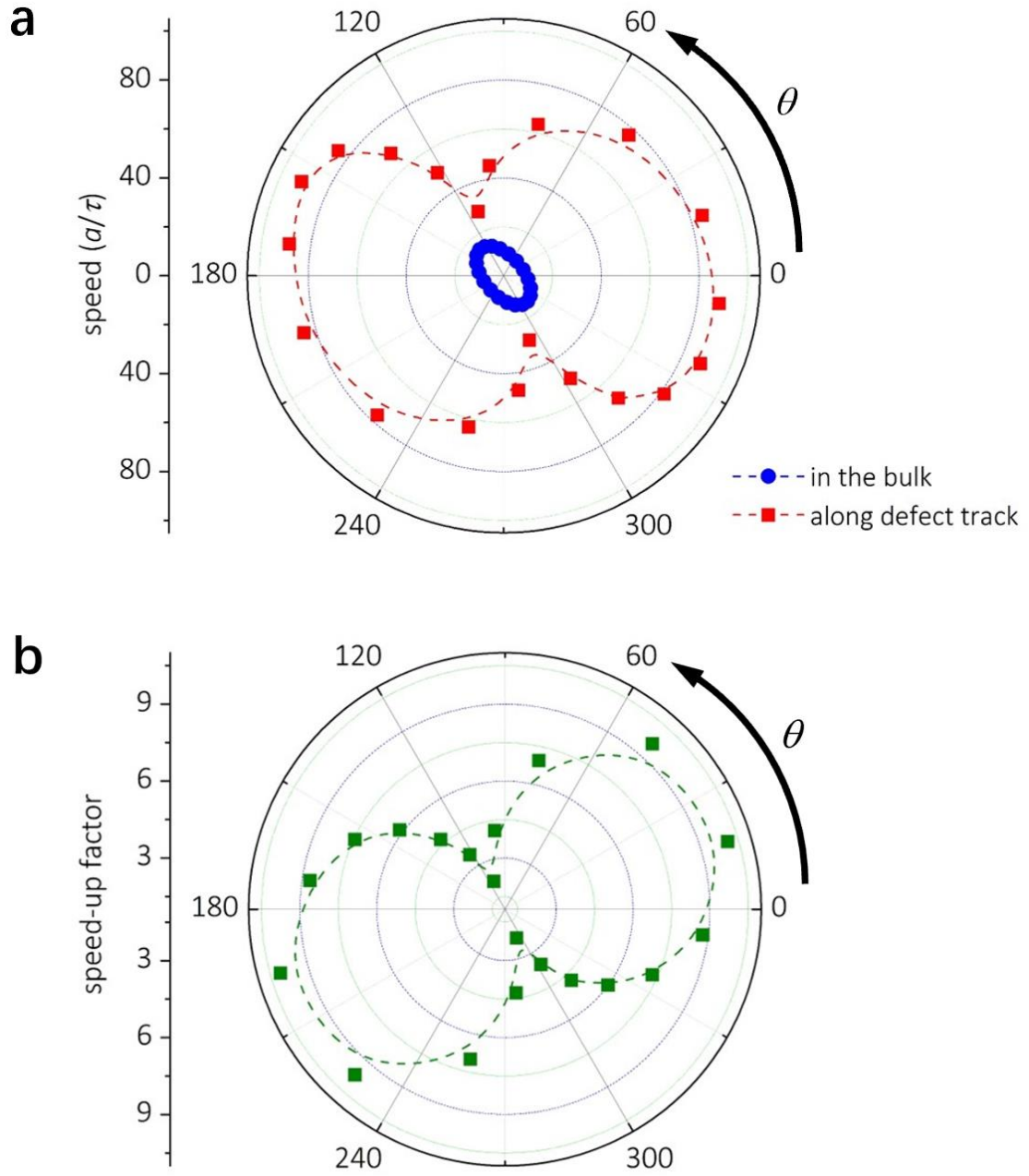


**Fig. S5 Polar plots of the skyrmion ratchet motion speed and speed-up factor along defect tracks //  $y$  under biharmonic in-plane magnetic fields  $H_x(t) = 0.003[\sin(\omega t) + \sin(3\omega t + \varphi)]$ . **a** Skyrmion ratchet motion speed and **b** speed-up factor as a function of skyrmion motion direction  $\theta$  in the bulk region.**

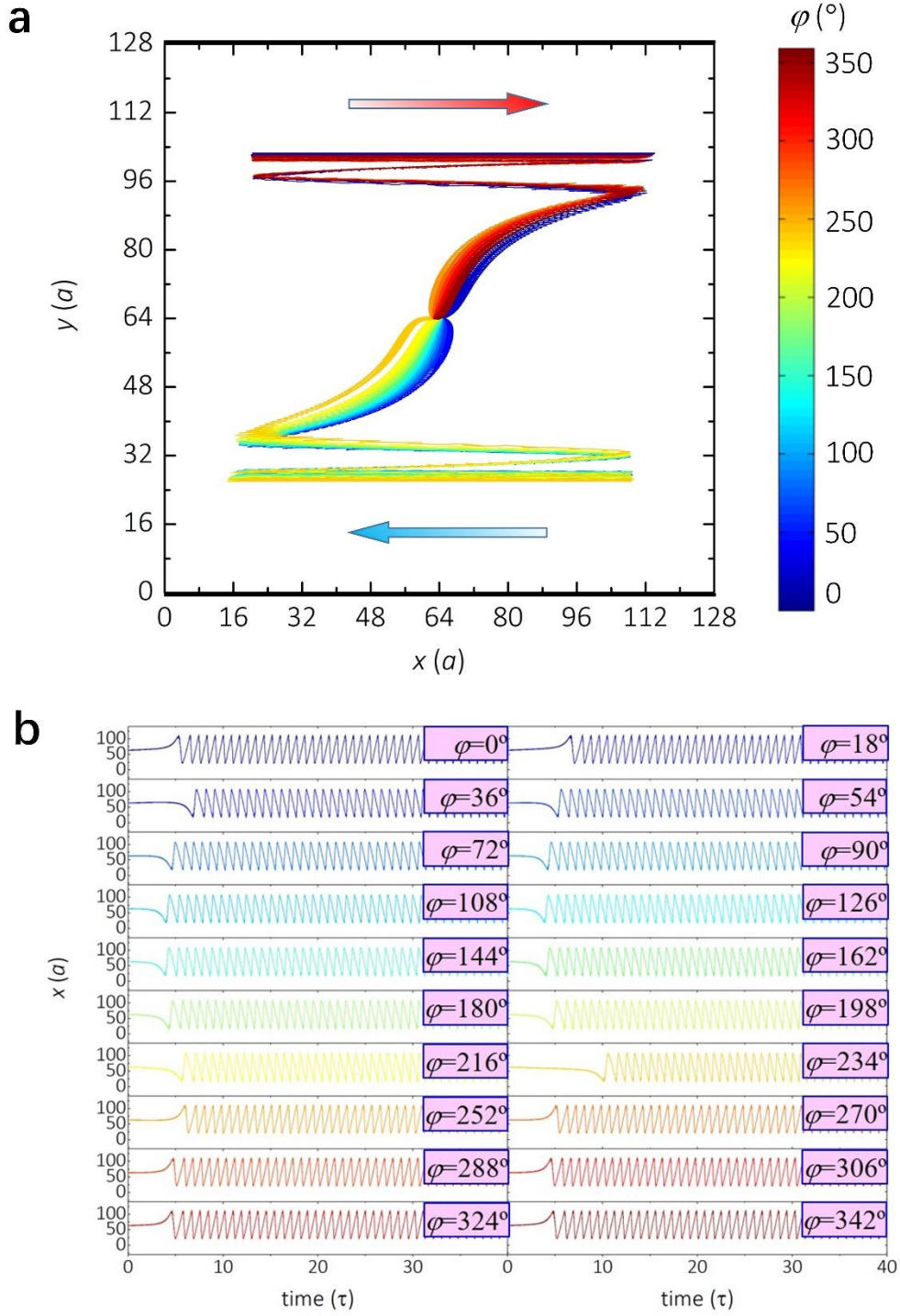


**Fig. S6 Ultrafast skyrmion ratchet motion along edges //  $x$  under biharmonic in-plane magnetic fields  $H_x(t) = 0.003[\sin(\omega t) + \sin(3\omega t + \phi)]$ .** **a** Trajectories of skyrmion ratchet motion at various phase  $\phi$  are plotted in different colors. **b** Long-time evolution curves of the position coordinate  $y_c$  of skyrmion ratchet motion at various phase  $\phi$ . The simulation box size is  $128a \times 128a$ , periodic along  $x$  direction and with two edges at  $y = 0a$  and  $y = 128a$ . For a given phase  $\phi$ , skyrmion is initially located at position  $(64a, 64a)$ .

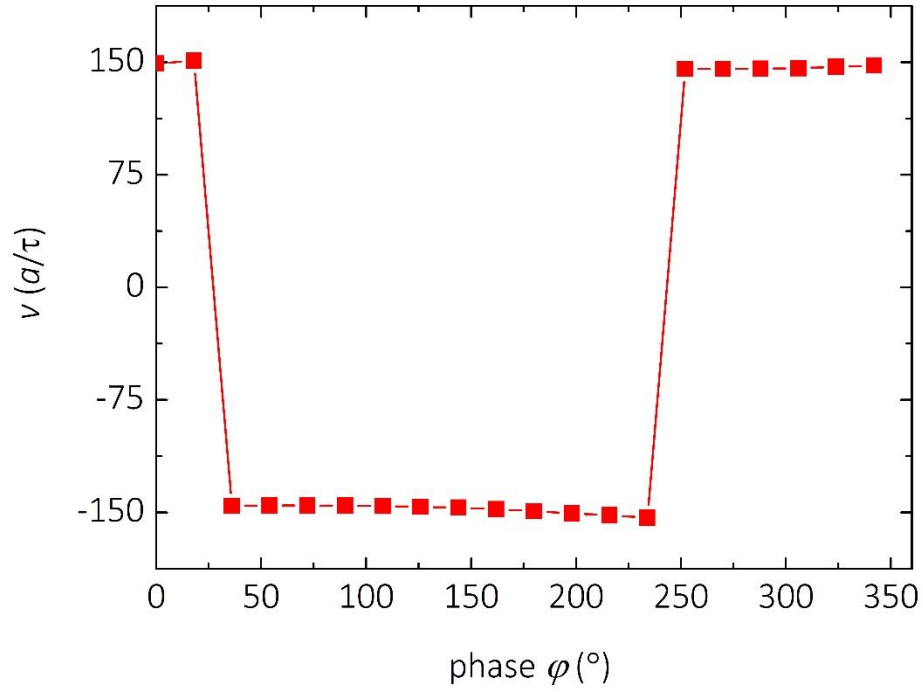


**Fig. S7** Skyrmion ratchet speed  $v$  as a function of phase  $\phi$  of the biharmonic field  $H_x(t) = 0.003[\sin(\omega t) + \sin(3\omega t + \phi)]$  for the case of “edge // y”.



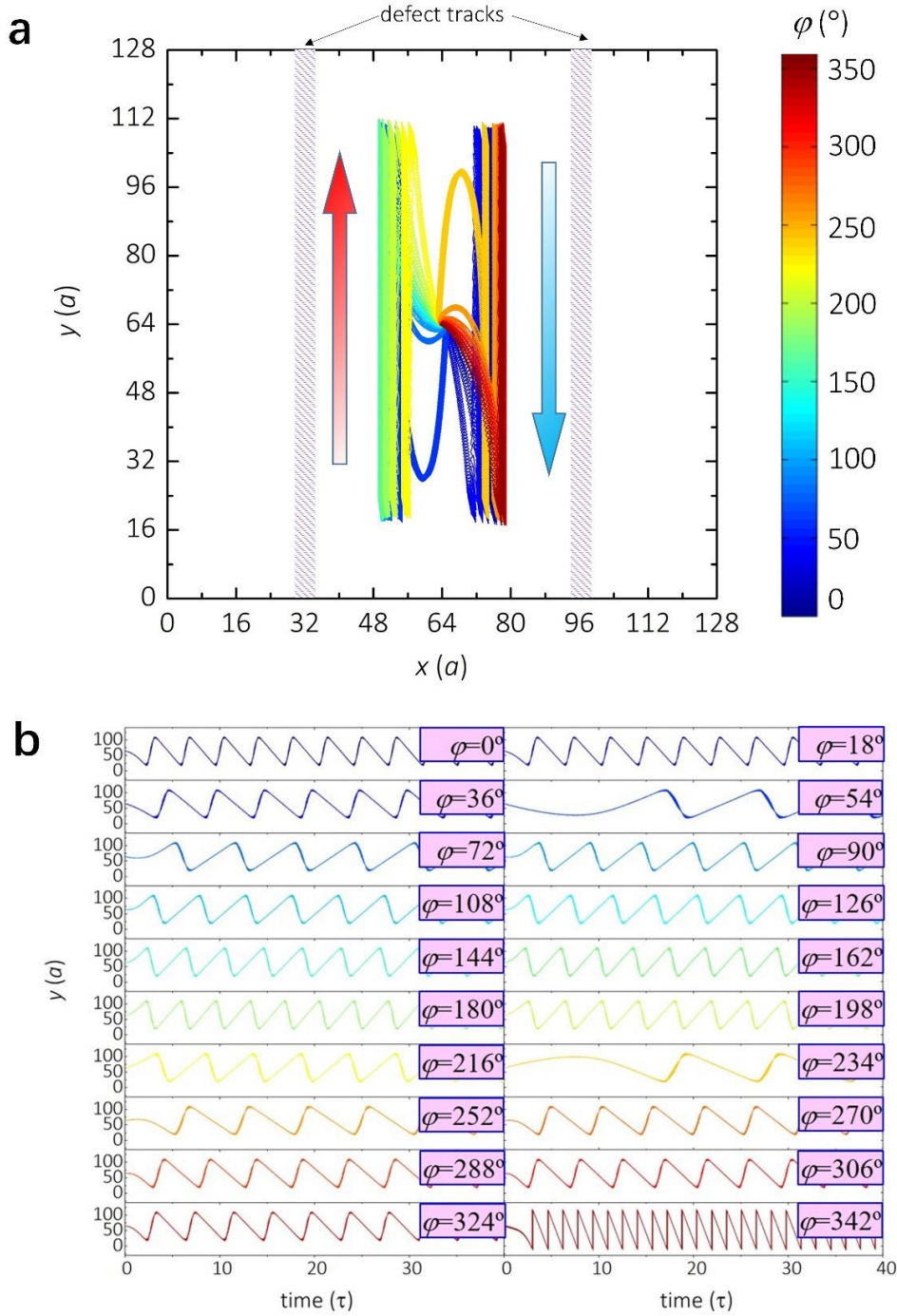


**Fig. S8 Skyrmion ratchet motion along defect tracks //  $y$  with a different exchange interaction from that of the bulk region under biharmonic in-plane magnetic fields  $H_x(t) = 0.003[\sin(\omega t) + \sin(3\omega t + \varphi)]$ .** **a** Trajectories of skyrmion ratchet motion at various phase  $\varphi$  are plotted in different colors. **b** Long-time evolution curves of the position coordinate  $y_c$  of skyrmion ratchet motion at various phase  $\varphi$ . In the simulation box, two  $4a$ -wide defect tracks (parallel to the  $y$ -axis) are located at  $x = 32a$  and  $x = 96a$ . The exchange interaction constant in the defect tracks is set to be half of that in the bulk region. For a given  $\varphi$ , the skyrmion is initially located at position  $(64a, 64a)$  and the skyrmion motion at the beginning can be considered as in the bulk region.

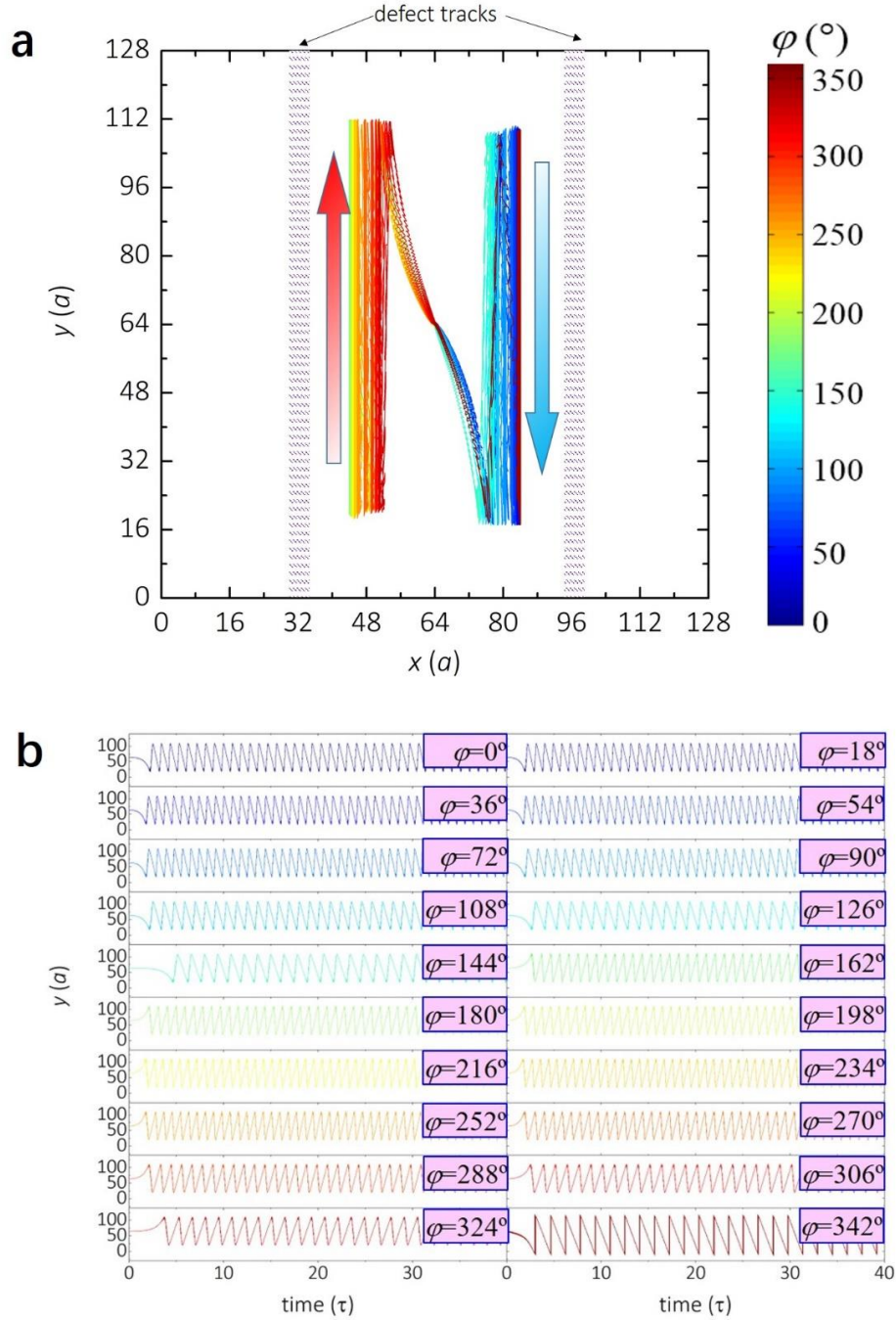


**Fig. S9 Skyrmion ratchet motion along defect tracks //  $y$  with a different anisotropy from that of the bulk region under biharmonic in-plane magnetic fields  $H_x(t) = 0.003[\sin(\omega t) + \sin(3\omega t + \varphi)]$ .** **a** Trajectories of skyrmion ratchet motion at various phase  $\varphi$  are plotted in different colors. **b** Long-time evolution curves of the position coordinate  $y_c$  of skyrmion ratchet motion at various phase  $\varphi$ . In the simulation box, two  $4a$ -wide defect tracks (parallel to the  $y$ -axis) are located at  $x = 32a$  and  $x = 96a$ . The PMA constant is set to be  $K=0.015$  in the defect tracks and  $K=0$  elsewhere. For a given  $\varphi$ , the skyrmion is initially located at position  $(64a, 64a)$  and the skyrmion motion at the beginning can be considered as in the bulk region.

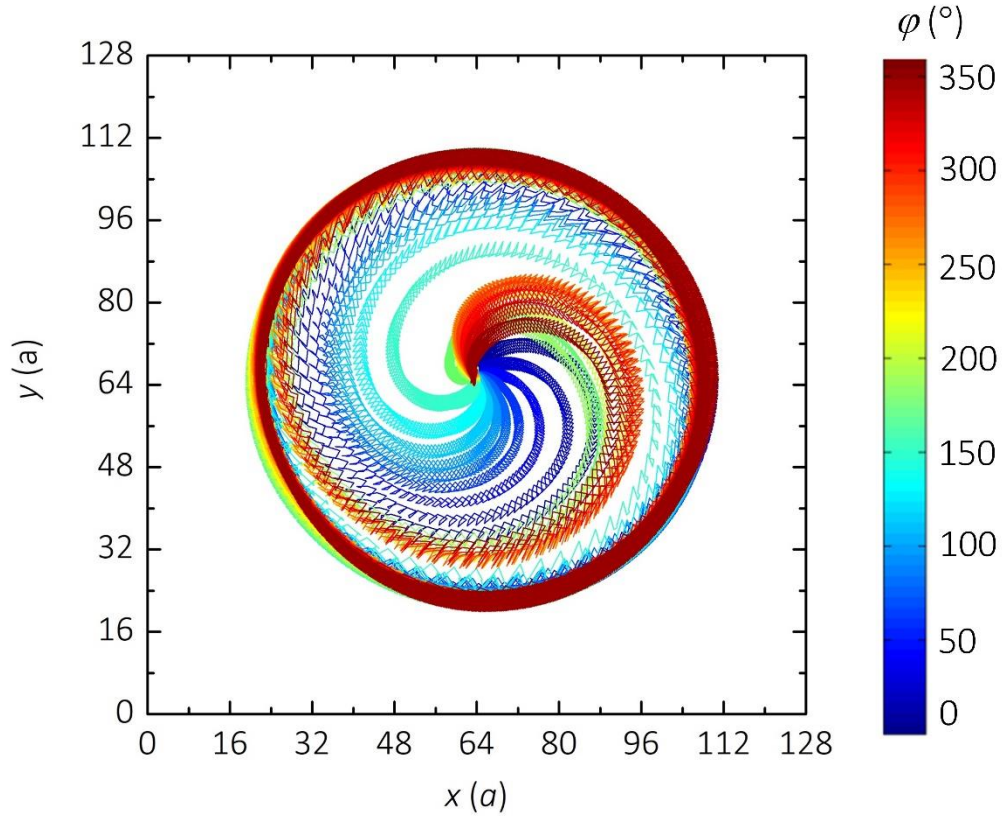


**Fig. S10 Ultrafast skyrmion ratchet motion on a circular disk under biharmonic in-plane magnetic fields  $H_x(t) = 0.003[\sin(\omega t) + \sin(3\omega t + \phi)]$ .** Trajectories of skyrmion ratchet motion at various phase  $\phi$  are given in different colors. The radius of the disk equal to  $64a$ . For a given  $\phi$ , the skyrmion is initially located at the center.

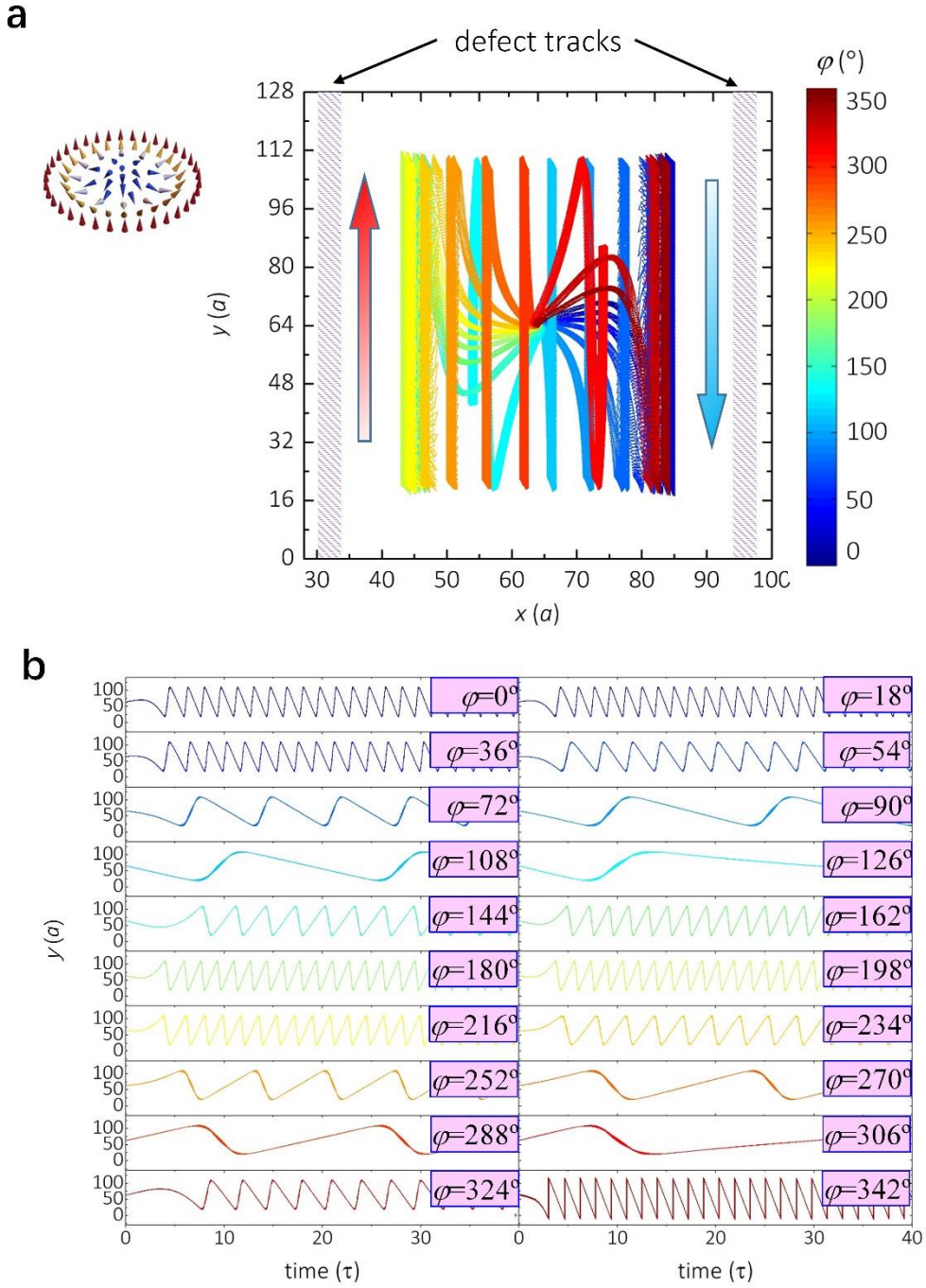


**Fig. S11 Ultrafast ratchet motion of Néel-type skyrmion along defect tracks //  $y$  under biharmonic in-plane magnetic fields  $H_x(t) = 0.003[\sin(\omega t) + \sin(3\omega t + \phi)]$ .** **a** Trajectories of skyrmion ratchet motion at various phase  $\phi$  are plotted in different colors. **b** Long-time evolution curves of the position coordinate  $y_c$  of skyrmion ratchet motion at various phase  $\phi$ . The simulation box size is  $128a \times 128a$ , periodic along  $x$  direction and with two edges at  $y = 0a$  and  $y = 128a$ . For a given phase  $\phi$ , skyrmion is initially located at position  $(64a, 64a)$ .